

**Minutes of splinter sessions held at the SPIRE Consortium Meeting  
2<sup>nd</sup> December 1998**

**Compiled by: Ken King**

1. Minutes of the Splinter Session for Institute Managers
2. Minutes of the Splinter Session on ICC Organisation
3. Minutes of Splinter Session on Simulations of SPIRE Observations
  - Confusion Noise in SPIRE Surveys
4. Minutes of Splinter Session on the Scientific Requirements Document
  - Time Sampling Interferograms with an LVDT
5. Minutes of Splinter Session on Detector Array Programme
6. Minutes of the FTS and Optics Splinter
  - Splinter Viewgraphs
  - New Proposal for SPIRE Optical Design
  - Impact of telescope defocus
7. Minutes of the Structure Team Splinter Meeting
  - New Mass and Thermal Dissipation Tables
  - Possible Conceptual Layout for the SPIRE Structure
8. Minutes of the Warm electronics & S/W working group splinter meeting
  - List of essential inputs required by the Warm Electronics and OBS Group

# Minutes of the Splinter Session for Institute Managers

Chairman: Ken King

Minutes prepared by: Ken King

## 1. WORK PACKAGES

The meeting discussed the need to define the SPIRE work packages in the near future, to allow the instrument implementation schedule to be defined. It will also provide milestones against which progress reporting can be made

**AI-MAN-0056-01:** King to send the template (for MS Word) for a work package description (based on the detector selection plan) to all local project managers.  
Due date: 4<sup>th</sup> Dec 1998.

**AI-MAN-0056-02:** Local project managers to complete the work package descriptions, as far as is possible. Due date: 15<sup>th</sup> Jan 1999.

**AI-MAN-0056-03:** Local project managers to send estimates of the length of time needed for manufacture of their AVM, CQM and PFM subsystems. These times should assume manufacture starts with the CDR (AVM and CQM) or CQM Readiness Review (PFM) and end with delivery of the subsystem to RAL for AIV.  
Due date: 11<sup>th</sup> Dec 1998.

## 2. REPORTING

The format of monthly reports to was discussed:

Monthly reports to ESA would be based on a template to be provided by ESA. This would require approximately a half page report by each Unit Manager (TBC). Local project managers will send their reports to the Unit Managers (with copy to King) on the last working day of each month.

The first report is assumed to be due at the end of January 1999.

Monthly reports would be based on milestones identified in the Instrument Implementation Schedule. This schedule and the list of milestones would be made available on the consortium WWW site.

**AI-MAN-0056-04:** King to provide a template (for MS Word) for the progress reports.  
Due date: 15<sup>th</sup> Jan 1999.

**AI-MAN-0056-05:** King to define a set of milestones covering the next six months.  
Due date: 22<sup>nd</sup> Dec 1998.

## 3. MANAGEMENT DOCUMENTATION

Drafts of the Product Tree, Documentation Tree and Work Breakdown Structure are required to be available to ESA by the managers meeting on 16<sup>th</sup> December. The local project managers will comment on a first version next week.

**AI-MAN-0056-06:** King to send drafts of the Product Tree, Documentation Tree and Work Breakdown Structure to local project managers.  
Due date: 4<sup>th</sup> December 1998.

**AI-MAN-0056-07:** Local project managers to send comments on the Product Tree, Documentation Tree and Work Breakdown Structure to King.  
Due date: 11<sup>th</sup> Dec 1998.

#### **4. PRODUCT ASSURANCE**

The current PA plan, issued with the SPIRE proposal needs to be reviewed and updated, before it can be agreed. Some names of the institute PA managers (mostly acting) were given.

**AI-MAN-0056-08:** Local project managers to send names of the Product Assurance responsible person at their institutes to King  
Due Date: 11<sup>th</sup> Dec 1998.

**AI-MAN-0056-09:** Local project managers/ PA managers to review the current PA Plan and make comments.  
Due date: 15<sup>th</sup> Jan 1999

#### **5. ICC**

The resources available for the development and implementation of the ICC is not clear.

**AI-MAN-0056-10:** Local project managers to provide a profile (year by year) of the effort available at their institute for ICC development work. An indication of the amount of time that these staff could spend at other institutes should also be made.  
Due date: 31 Jan 1999.

# Minutes of the Splinter Session on ICC Organisation

**Chairman: Ken King**

**Minutes prepared by: Ken King**

The purpose of the meeting was to discuss the role, membership and tasks of the ICC Definition Team as proposed by the SPIRE Steering Group.

It was agreed that the role of this team was to provide the scientific and technical input required to define and implement the ICC work packages.

The membership should be:

- An ICC Scientist - who would lead the team.
- The ICC and DAPSAS centre managers
- The Ground Segment Systems Scientist

plus other scientists and technical staff with experience of ground segment and data processing systems.

A list of contact points/potential members from the institutes present at the meeting was drawn up:

Stockholm	H-G Floren
Padova	A Franceschini
IFSI	P. Saraceno
ATC	G. Wright
IAS	P. Cox, F. Pajot
IAC	I Perez-Fournon
ICSTM	N. Todd, S, Coe
LAS	J-P Baluteau
SAP	J-L Augueres, R. Gasteau

In the light of the number of people identified it was thought that the ICC Definition Team would have to form sub groups to work on specific tasks.

The ICC Scientist, who was not identified, would organise a kick-off meeting of the Team in mid to late January.

The following tasks of the team were identified at the meeting:

- To refine the work packages for the implementation and maintenance of the data processing software to allow the ICC Steering Group to allocate these to the appropriate ICC Centres.
- To advise members of the FIRST/Planck Commonality Working Groups which deal with ICC matters, on the SPIRE inputs.

# Minutes of Splinter Session on Simulations of SPIRE Observations

Chairman: Laurent Vigroux

Minutes prepared by: Matt Griffin

A revised version (V0.2) of the document *Confusion Noise in SPIRE Surveys* by Aussel, Vigroux and André was presented by Laurent, including some results (the note is attached to these minutes). The updated model incorporates the comments made in the note of September 13 by Griffin Bock and Gear (*Comments on the note Confusion noise in SPIRE surveys*) but there are still some points that need to be clarified and discussed.

## Actions

Due dates for all of these: end December (at the very latest) except where otherwise stated, so that the information can be used to produce a revised version of the model in January.

<b>AI-SIM-0056-01</b>	Review revised document and send comments to Laurent and Matt	All
<b>AI-SIM-0056-02</b>	Investigate incorporation of AOCs model (including pointing jitter)	LV
<b>AI-SIM-0056-03</b>	Extend the model to include more realistic sky by - having the same set of sources in the artificial sky maps at all of the wavelengths by selecting objects from the z-L plot) - incorporating clustering	LV/AF/SJO
<b>AI-SIM-0056-04</b>	Provide information on the PSF from the optical model and its variation across the field (Jan. 31)	BMS
<b>AI-SIM-0056-05</b>	Study consequences of chopping for confusion-limited imaging	SJO
<b>AI-SIM-0056-06</b>	Make the model sky maps available electronically so that people try different source extraction algorithms.	LV
<b>AI-SIM-0056-07</b>	Consider the definition of quantitative figures of merit for confusion-limited observations	AF
<b>AI-SIM-0056-08</b>	Produce a revised version of the model based on the above (to be presented and reviewed at the next Detector Array meeting) (Jan. 16)	LV
<b>AI-SIM-0056-09</b>	Other (lower priority) areas in which the model can be made more representative are: - include observing overheads explicitly - include ability to simulate non-Gaussian noise contributions (End Feb.)	LV

LV = Laurent Vigroux  
AF = Alberto Franceschini  
SJO = Seb Oliver  
BMS = Bruce Swinyard

# Confusion noise in SPIRE surveys

## Version 0.2

H. Aussel, L. Vigroux, P. André  
 Service d'Astronomie, CE-Saclay, DSM/DAPNIA,  
 Bat 709, Orme des Merisiers, CE-Saclay,  
 F-91191 Gif-sur-Yvette Cedex

November 30, 1998

### Abstract

We present a simplified model of extragalactic surveys with SPIRE, the Spectral and Photometric Imaging REceiver on board of FIRST, performed at 250  $\mu\text{m}$  and 500  $\mu\text{m}$ , in order to study the impact of confusion noise. We show on preliminary simulations that confusion is the major issue for dealing with extragalactic source extraction.

*Note* : Some of the remarks of the note of the 26 October 1998 by Griffin, Oliver and Gear have been taken into account.

## Introduction

This report address the problem of confusion noise for SPIRE, the FIRST bolometer instrument, for its survey mode. Indeed, confusion could be the main limitation of the instrument, due to the high number of extragalactic sources per square arc degree that are predicted by various number counts models. In order to investigate the problem of confusion, we have developed a very simplified model of a SPIRE survey and we have simulated observations at 250  $\mu\text{m}$  and 500  $\mu\text{m}$  with two kind of detectors : square pixel matrix of bolometers and array of horns (back-up option). We describe in section 1 the model we have used.

## 1 The model.

### 1.1 Model for source fluxes and positions

To model the sky as observed in SPIRE surveys, we have used two of number counts models presented in [1], namely the number counts model of Franceschini et al. (1997) [2], and the one of Rowan-Robinson (1998) [4], because they are two extreme models from the point of view of the predicted source density, the counts predicted by the model developed by Guiderdoni et al. (1998) [3] lay between the values predicted by the two others.

Each model result is a function that gives the number  $N$  of sources brighter than a given flux  $S$  per square degree as a function of  $S$ . The derivative of this function  $N(> S)$  is the number of sources  $dN$  with a flux  $s \in [S, S + dS]$ , multiplied by a factor  $-1$ . If one consider only a given flux range,  $[S_l, S_u]$ , one can build a function  $f$ , that gives the number of sources per square degree *dimmer* than a given flux  $S$

and brighter than  $S_l$  :

$$f(S) = \int_{S_l}^S dN(s)ds \quad (1)$$

If one consider now the function  $F(S)$  defined by :

$$F(S) = \begin{cases} 0 & \text{if } S < S_l, \\ \frac{f(S)}{f(S_u)} & \text{if } S_l < S < S_u, \\ 1 & \text{if } S > S_u. \end{cases} \quad (2)$$

The function  $F$  grows from 0 to 1 when  $S$  varies between  $]-\infty, +\infty[$ . In this sense,  $F(S)$  can be interpreted as the *partition function* of the random variable  $X_S$ , the flux of a source. We can therefore build a random flux generator, that follows the number counts model, by computing the function  $F$  and using the classical computer implemented uniform generator. The random variable  $X = F^{-1}(U)$ , where  $U$  is a random variable following the uniform law, will have  $F$  as partition function.

To simulate a given area of sky  $A$ , the models predict that the number of sources brighter than  $S_l$  will be  $n = A \times N(> S_l)$ . We work on an area large enough so that poissonian fluctuations ( $\propto 1/\sqrt{n}$ ) can be neglected.

We choose to simulate an area of 400 square arc minutes, where the number of sources brighter than 15  $mJy$  is roughly of 130, according to the Franceschini model. For our simulations, we choose  $S_l = 100 \mu Jy$  and  $S_u = 10 Jy$ . This  $S_l$  value gives a number  $N$  of sources in our simulation of 16746, with the Franceschini model,  $N = 6822$  with the Rowan-Robinson model.

The fluxes of the sources are generated with our random flux generator. The counts obtained from the simulated sets are shown in figure 1 for the various models. The positions in the images are generated by using a uniform generator.

## 1.2 Simulation of the focal plane

Once the positions and fluxes of the sources are known, we compute a oversampled image of the focal plane of FIRST. The resolution choosed for the computations is 0.5 arcsec, allowing for a good accuracy of the computations, since the smallest pixel size of SPIRE to be considered is 9 arcsec.

We assume an ideal telescope *i.e.* a single circular aperture. Therefore, the intensity of the diffraction limited image of a point source (PSF) is :

$$I = I_0 \left[ \frac{J_1(m)}{m} \right]^2 \quad (3)$$

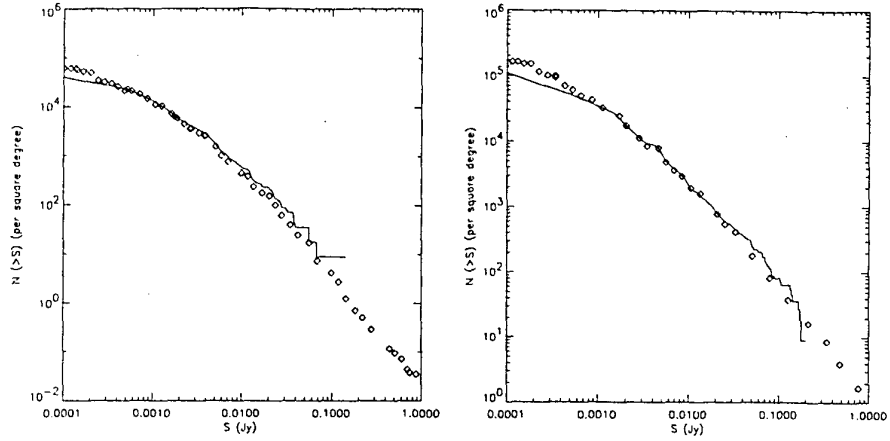
where  $J_1$  is the Bessel function and with :

$$m = \frac{\pi a i}{\lambda} \quad (4)$$

where  $a$  is the telescope aperture ( $a = 3.5m$ ),  $\lambda = 250 \mu m$  or  $\lambda = 509 \mu m$  is the wavelength, and  $i$  is the incidence angle (we use the approximation of small angles).

We have computed PSF with a resolution of 0.5 arcsec on the focal plane, on an area of  $240 \times 240$  arcsec. An image of  $20 \times 20$  arcmin with a resolution of 0.5 arcsec is computed by adding one PSF multiplied by the flux for each sources.

Figure 2 presents two simulated fields from each of the two models used.



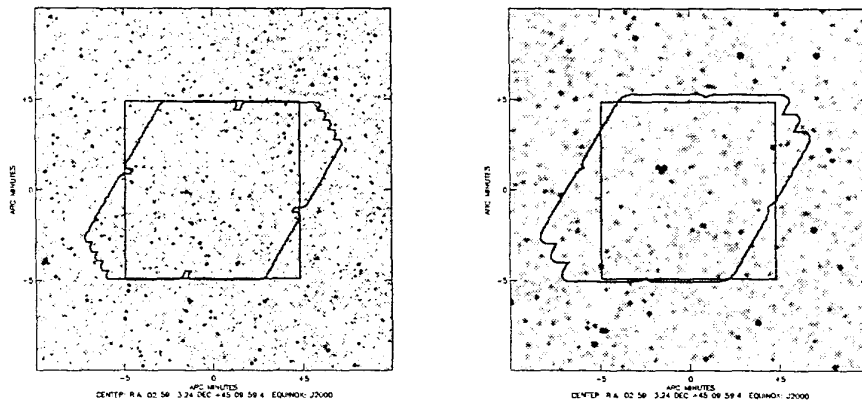
(a)  $\lambda = 250 \mu\text{m}$  counts model from Rowan-Robinson (1998)[4]

(b)  $\lambda = 250 \mu\text{m}$  counts model from Franceschini et al. (1997)[2]

Figure 1: Comparison of the counts obtained with the simulated fluxes with the models.

Line : counts derived from the simulation of a 400 arcmin area.

Diamonds : predictions of the model



(a)  $\lambda = 250 \mu\text{m}$  counts model from Franceschini et al. (1997)[2]. Upper cut is 0.2 mJy/arcsec<sup>2</sup>.

(b)  $\lambda = 500 \mu\text{m}$  counts model from Franceschini et al. (1997)[2]. Upper cut is 0.1 mJy/arcsec<sup>2</sup>.

Figure 2: Simulated images of a  $20 \times 20$  arcmin area of the sky, as observed at the focus of FIRST telescope at  $250 \mu\text{m}$  with a resolution of 0.5 arcsec. The images are displayed with a resolution of  $2 \times 2$  arcsec. At  $500 \mu\text{m}$ , confusion is already a problem for faint fluxes with the Franceschini et al. (1997) [2] model (b) at the resolution of the display, that is four times broader than the resolution of the computations. The area surveyed with option 1 and 2 (squares) and option 3 are outlined.



Option	$\lambda_{obs}$	Pixel size	Number of pixels
1 ( $F\lambda$ )	250 $\mu\text{m}$	18"	16 $\times$ 16
	500 $\mu\text{m}$	36"	8 $\times$ 8
2 ( $F\lambda/2$ )	250 $\mu\text{m}$	9"	32 $\times$ 32
	500 $\mu\text{m}$	18"	16 $\times$ 16
3 ( $2F\lambda$ )	250 $\mu\text{m}$	36"	61
	500 $\mu\text{m}$	72"	19

Table 1: Detailed parameter of the detectors.

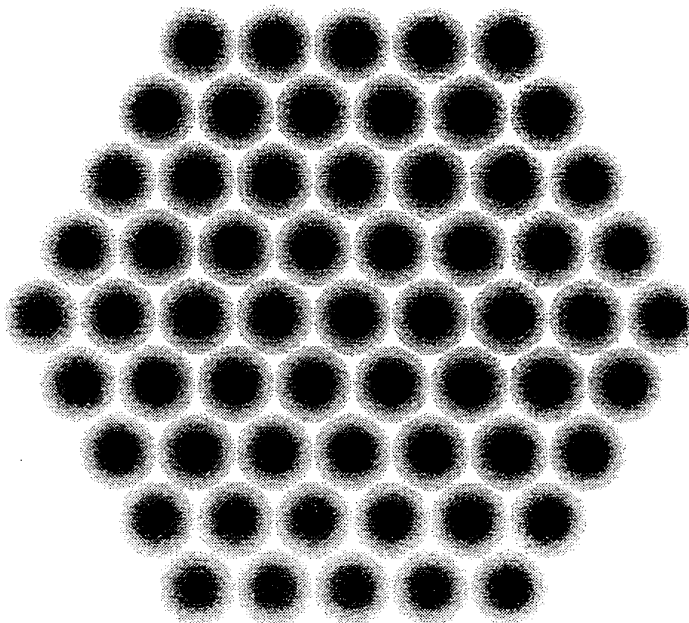


Figure 3: Image of the response of the 61 horns bolometers array

### 1.3 Simulation of the detectors

We have considered three kind of detectors summarized in table 1 :

1. array of 16  $\times$  16 square pixels of  $F\lambda$  of size, *i. e.* 18 arcsec at 250  $\mu\text{m}$ , and 8  $\times$  8 pixels of 36 arcsec at 500  $\mu\text{m}$ . The pixels are contiguous and their response is constant over the whole pixel.
2. array of 32  $\times$  32 square pixels of  $F\lambda/2$  of size, *i. e.* 9 arcsec at 250  $\mu\text{m}$ , and 16  $\times$  16 pixels of 18 arcsec at 500  $\mu\text{m}$ . The pixels are contiguous and their response is constant over the whole pixel.
3. array of 61 bolometers horns (backup option). The horns hexagonally placed and separated by  $2F\lambda$ . Their response is a gaussian of  $F\lambda$  FWHM. Figure 3 present a image of the array response.

The calculated image of the survey is projected on the detector, to simulate each pointing of the raster for cases 1 and 2, or of a jiggling map for case 3.

In SPIRE, we have taken two sources of noise into account :

1. detector noise with Noise Equivalent Power (NEP) equal to [1] :  
 $NEP_{det} = 3 \times 10^{-17} W.Hz^{-1/2}$

2. photon noise  $NEP_{ph}$ , that is dominated by the telescope itself.

The photon Noise Equivalent Power is computed from the RMS fluctuation  $(\Delta n)^2$  of the number  $n$  of photon of a black body that arrive on the detector [5]. Thus we have:

$$(\Delta n)^2 = n(n + 1) \quad (5)$$

The photon emission is dominated by the telescope, with emissivity  $\epsilon$  and temperature  $T = 80$  K [1]. Last, this energy is received by a bolometer with quantum efficiency  $\eta_{bol}$ , with a telescope of collecting area  $A_t$  seeing the pupil under the solid angle  $\Omega$ , in the frequency range  $\Delta\nu$ , through an optic with efficiency  $\eta_{opt}$ . The fluctuation of the number  $N$  of photon arriving on the detector is therefore :

$$(\Delta N)^2 = \epsilon \eta_{bol} \eta_{opt} N (1 + \epsilon \eta_{bol} \eta_{opt} N) = \frac{\epsilon \eta_{bol} \eta_{opt}}{e^{\frac{h\nu}{kT}} - 1} \left( \frac{\epsilon \eta_{bol} \eta_{opt}}{e^{\frac{h\nu}{kT}} - 1} + 1 \right) \quad (6)$$

Each photon has an energy  $h\nu$  and the density of states it can occupy is :

$$d = 2 \times \frac{2h\nu^3}{c^2} \quad (7)$$

Therefore we have :

$$NEP_{ph}^2(\lambda) = A_t \Omega \int_{\Delta\nu} 2 \times \frac{2h\nu^3}{c^2} (h\nu) \frac{\epsilon \eta_{bol} \eta_{opt}}{e^{\frac{h\nu}{kT}} - 1} \left( \frac{\epsilon \eta_{bol} \eta_{opt}}{e^{\frac{h\nu}{kT}} - 1} + 1 \right) d\nu \quad (8)$$

We have for SPIRE [1] :

$$A_t \Omega = \alpha \lambda^2 \quad T_{tel} = 80K \quad \epsilon_{tel} = 0.04 \quad (9)$$

$$\eta_{opt} = 0.3 \quad \eta_{bol} = 0.8 \quad \Delta\lambda = \frac{\lambda}{3} \quad (10)$$

The value of  $\alpha$  depends on the configuration, taking into account Lyot spot and area of the bolometer. Following [6], we take for option 3  $\alpha = 0.8$  so that  $A_3 \Omega_3 = 0.8 \lambda^2$ . For square pixels,  $\Omega = \pi/4F^2$  [6] is the same (the telescope has the same optical configuration) and the collecting area are  $A_1 = (F\lambda)^2$  and  $A_2 = (F\lambda)^2/4$ , where  $F$  is the focal length of the telescope.

The total noise equivalent power of the bolometer  $NEP_{tot}$  is then :

$$NEP_{tot} = \sqrt{NEP_{ph}^2 + NEP_{det}^2} \quad (11)$$

If one observes a point source radiating with the flux density  $S_{\nu,s}$ , assumed to be constant over  $\Delta\nu$ , the bolometer receives the power :

$$P_b = S_{\nu,s} A_t \Delta\nu \eta_{tel+det} \eta_{pix} \quad (12)$$

where  $\eta_{pix}$  is the portion of the PSF intercepted by the bolometer,  $\eta_{tel+det}$  is the overall efficiency of the instrument and telescope. We have :

$$\eta_{tel+det} = \eta_{opt} \eta_{bol} \eta_{chop} \quad (13)$$

		option 1 $\alpha = \pi/4 = 0.785$	option 2 $\alpha = \pi/16 = 0.196$	option 3 $\alpha = 0.8$
Wavelength	Noise	NEP ( $10^{-17} W.Hz^{-1/2}$ )	NEP ( $10^{-17} W.Hz^{-1/2}$ )	NEP ( $10^{-17} W.Hz^{-1/2}$ )
250 $\mu m$	photon	9.06	4.53	9.14
	detector	3.00	3.00	3.0
	total	9.54	5.43	9.62
500 $\mu m$	photon	5.05	2.53	5.10
	detector	3.00	3.00	3.00
	total	5.88	3.92	5.92
Wavelength	Noise	r.m.s. (mJy)	r.m.s. (mJy)	r.m.s. (mJy)
250 $\mu m$	total	0.63	0.36	0.63
500 $\mu m$	total	0.77	0.52	0.78

Table 2: Noise equivalent power and noise level ( $1 \sigma/\text{pixel}$ ) for simulation of 15 min exposures.

where  $\eta_{chop} = 0.45$  is the chopping efficiency and  $A_t = \pi 3.29^2/4$  [1].

If this sources is observed during the time  $t$ , the noise reduces as  $\sqrt{t}$  and the signal over noise ratio is therefore :

$$S/N = \frac{S_{\nu,s} A_t \Delta\nu \eta_{tel+det} \eta_{pix}}{\frac{NEP_{tot}}{\sqrt{2\eta_{obs}t}}} \quad (14)$$

Note that the observing time has been multiplied by a factor  $\eta_{obs}$ , the observation efficiency, to take into account the overheads *i. e.* that not all the time dedicated to the observation is used to take data.

The equation 14 allow to compute the signal over noise for the detection of a point source. In our case, we are interested in computing the noise level in one pixel. Thus, we have to consider for this purpose the observation of a constant extended source and use the following equation :

$$S/N = \frac{S_{\nu,s} A_t \Delta\nu \eta_{tel+det}}{\frac{NEP_{tot}}{\sqrt{2\eta_{obs}t}}} \quad (15)$$

where  $\eta_{pix}$ , the pixel efficiency, that is the average flux recieved by a pixel when observing a source, is no longer taken into account.

Setting  $S/N$  to 1 in equation 15 gives us the flux density r.m.s. of the noise, which, in this case is equal to  $S_{\nu,s}$ .

Values of  $\alpha$  and NEPs are summarized in table 2. Note that we assume that the noise is independant of the simulated sources, because we assume that photon noise due to the sources is neglectible against those of the background and telescope.

Once the projection of one pointing (raster step or jiggling step) has been computed, a gaussian noise with r.m.s. corresponding to the option and wavelength is added to the image.

#### 1.4 Map reconstruction

Once each image (*i.e.* the flux collected by each bolometer for a given pointing) has been computed, they are coadded in a "raster" or "jiggle" map. We follow for this

the prescriptions of the IRAM reduction package NIC [7]. Each pointing is added to the raster map with a weight  $W$  :

$$W = \left( \frac{\sin(ud)}{ud} \right)^2 T \quad (16)$$

$$u = \frac{2\pi D}{\lambda} \quad (17)$$

where  $d$  is the distance between the position of the final map and the center of the bolometer and  $T$  is the value of the transfer function of the bolometer at this point. A noise map is also produced, using  $W^2$  as weight.

The map of the observation is then interpolated on a regular RA-DEC oriented grid using bilinear interpolation. In option 3, where directions of the “jiggling” are not perpendicular, care has been taken to have a flux conservative reprojection.

## 2 Results

The model described in the previous section has been used to simulate survey observations with the three kind of detectors. Due to SPIRE design the three (of which two are simulated) are observed at the same time. This means that the same pointings and same integration time are used for the two channels. To fully sample the PSF at the longest wavelength, one has to scan the sky by steps of  $\lambda/2$  in both axis. This leads to a scan in only  $\lambda$  for the shortest wavelength thus leading to an undersampled map. Thus the minimal sampling rate is  $\lambda/2$  at  $250 \mu\text{m}$  that gives  $\lambda/4$  at  $500 \mu\text{m}$ . Together with this minimal sampling, we have simulated oversampled maps at  $\lambda/4$  at  $250 \mu\text{m}$  and  $\lambda/8$  at  $500 \mu\text{m}$ .

While the shortest wavelength commands the raster or jiggle step size, the longest wavelength commands the number of steps : the bolometer size has to be fully covered in order to obtain an homogeneous map. If a  $\lambda/2$  step at  $250 \mu\text{m}$  requires  $4 \times$  steps to obtain a full coverage of the PSF at  $250 \mu\text{m}$ , this translate to  $\lambda/4$  at  $500 \mu\text{m}$ . Thus, a  $8 \times 8$  map is in fact required.

### 2.1 Observations

In order to ensure a proper comparison of the three detector, we have simulated observations of an area of *fixed surface* within a *fixed total observation time* at a *fixed resolution*. The area for each configuration is  $100 \text{ arcmin}^2$ , except for option 3 (2 FL horns) at  $500 \mu\text{m}$  where the 27 horns cover a slightly larger surface giving a total area of  $113 \text{ arcmin}^2$ . To cover at  $\lambda/4$  and  $250 \mu\text{m}$  this area, 4 “jiggle” maps of 64 pointings each are required. We set the observing time to 64 minutes, giving an exposure time of 15 seconds per pointings in this configuration. The exposure time per pointing for each other options were computed to fill the same total observing time. For exemple, an array of  $16 \times 16$  square pixels of  $18''$  can map the same area in the same time and stay  $60''$  at each pointing, with 4 raster maps with half a pixel steps.

The detectors are detailed in table 1 and the observations are detailed in table 3

### 2.2 Images

Figures 4, 5 and 6 present the images obtained at  $250 \mu\text{m}$  and  $500 \mu\text{m}$  with the low resolution and high resolution mode, on the field simulated with Franceschini et al. number counts [2]. Figures 4, 5 and 6 present the same results for Rowan-Robinson number counts [4]. Note that we had to modify the lower cut of option 3 results

Option	Resolution at 250 $\mu\text{m}$	Number of pointings	Exposure time	Covered area	Total time
1( $F\lambda$ )	$\lambda/2$	$4\times 4\times 4$	1 min	100	1.07
	$\lambda/4$	$8\times 8\times 4$	0.25 min	100	1.07
2 ( $F\lambda/2$ )	$\lambda/2$	$2\times 2\times 4$	4 min	100	1.07
	$\lambda/4$	$4\times 4\times 4$	1 min	100	1.07
3 ( $2F\lambda$ )	$\lambda/2$	$8\times 8\times 4$	0.25 min	100	1.07
	$\lambda/4$	$16\times 16\times 4$	0.0625 min	100	1.07

Table 3: Details of the simulated observations. For each option, the step size (resolution) at 250  $\mu\text{m}$  is given, as well as the number of pointing required for a complete coverage at 500  $\mu\text{m}$ . The number of pointings is given in the following way :  $N_{step_1} \times N_{step_2} \times N_{raster}$  where  $N_{raster}$  is the number of independant raster or jiggle maps needed to cover the area.

to leave some dynamics in the image. Indeed, lower cut is 10  $\sigma$  while it is 1  $\sigma$  for options 1 and 2.

It is clear from the output images that confusion dominates all the maps for source extraction. With option 3 ( $2F\lambda$  horns), only a few pixels are below the 1  $\sigma$  level, at the edge of the map where redundancy is small, and most of the pixel are *above* the usual 3  $\sigma$  level used for source detection. Moreover, many sources appear blended together, whatever the detector being used.

Depending on the kind of observations and the detector, the effects of confusion are more or less severe :

- The mapped obtained at a better resolution are less affected.
- The smaller the pixels, the less prominent is confusion at high flux level.

When dealing with exposures as long as the ones simulated, the detector and photon noise originating from the telescope mirror become neglectibles, especially for large pixels.

Two ways can be though to overcome the confusion problem :

- use pixels as small as possible to fight this effect, but big enough to avoid to be dominated by instrument noise.
- observe with scan maps rather than pointed “jiggle” maps, in order to obtain a high resolution on the final map. This is only possible if the relative pointing accuracy and control of the satellite is good.

Two techniques are usually used detect sources against confusion : the deconvolution and the P(D) analysis. Both require a good understanding of the instrumental noise, as well as accurate measures of the beam profile, that are difficult to obtain, especially when the the intrument is very sensitive.

### 3 Conclusion

We have presented a simplified model of extragalactic surveys with SPIRE, the Spectral and Photometric Imaging REceiver on board of FIRST, performed at 250  $\mu\text{m}$  and 500  $\mu\text{m}$ , in order to study the impact of confusion noise. We show on preliminary simulations that confusion is the major issue for dealing with extragalactic source extraction. We show that a detector made of small pixel ( $F\lambda/2$ ) is

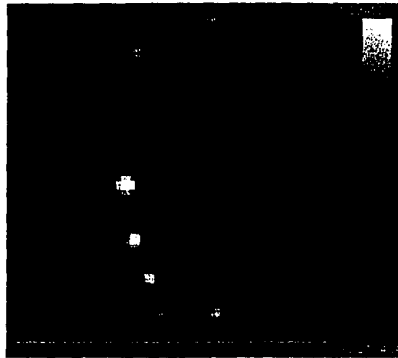
less sensitive to this problem. Observations obtained with very small steps between pointings or scan technique are also preferred.

Beyond the scope of extragalactic surveys, the problem rises the question of finding a good “empty” place when using chopping techniques. The probability of finding a source bright enough to be above the noise level for in any part of the sky is large, even for short exposures.

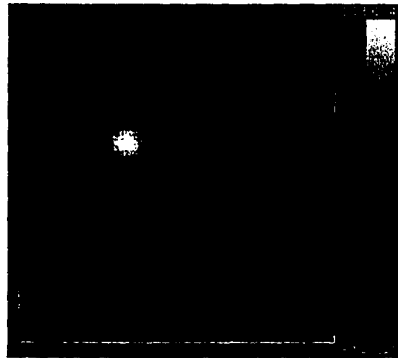
This study will be extended to take into detectors closer to reality : non homogenous response of the pixels, pixels with filling factor lower than one, *etc...* Moreover, tests of P(D) and deconvolution will be done to analyse the outputs of the simulations.

## References

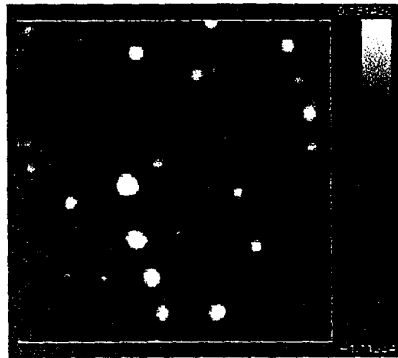
- [1] Griffin M., and the SPIRE consortium, 1998, “SPIRE, a bolometer instrument for FIRST”, A proposal to the European Space Agency
- [2] Franceschini A., Aussel H., Bressan A. *et al.*, 1997, “Sources counts and background radiation”, in *The Far Infrared and Submillimeter Universe*, ESA SP-401
- [3] Guiderdoni B., Hivon E., Bouchet F., Maffei B., 1998, MNRAS, 295,877
- [4] Rowan-Robinson M., 1998, MNRAS *in press*
- [5] Rohlfs K., Wilson L. T., 1996, “Tools of Radio Astronomy”, second edition, Springer
- [6] Griffin M., Bock J., Gear W., “Comparison of sensitivities of 0.5F $\lambda$ , 1.0F $\lambda$  and 2.0F $\lambda$  arrays for the BOL”, Note no. BOL/QMW/N/0026.10
- [7] D.Broguière, R.Neri, A.Sievers, NIC Bolometer Users Guide, Version 1.4-01, <http://irau2.iram.fr/GS/nic/nic.html>



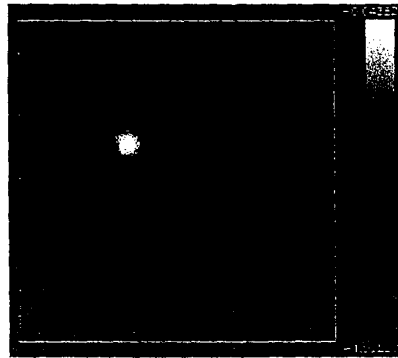
(a)  $\lambda = 250 \mu\text{m}$ ; resolution of  $\lambda/2$ . Display is  $\text{Log}(f \text{ mJy/pixel})$ . Lower cut is  $1\sigma$ , upper cut is  $20\sigma$ .



(b)  $\lambda = 500 \mu\text{m}$ , resolution of  $\lambda/4$ . Display is  $\text{Log}(f \text{ mJy/pixel})$ . Lower cut is  $1\sigma$ , upper cut is  $40\sigma$ .

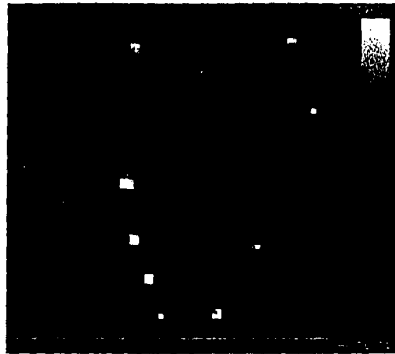


(c)  $\lambda = 250 \mu\text{m}$ , resolution of  $\lambda/4$ . Display is  $\text{Log}(f \text{ mJy/pixel})$ . Lower cut is  $1\sigma$ , upper cut is  $20\sigma$ .

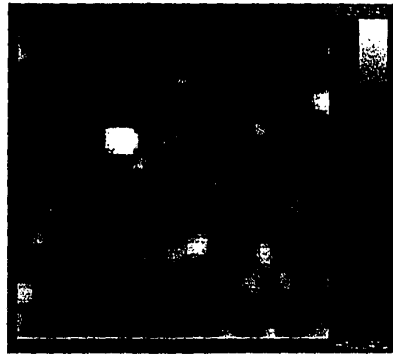


(d)  $\lambda = 500 \mu\text{m}$ , resolution of  $\lambda/8$ . Display is  $\text{Log}(f \text{ mJy/pixel})$ . Lower cut is  $1\sigma$ , upper cut is  $40\sigma$ .

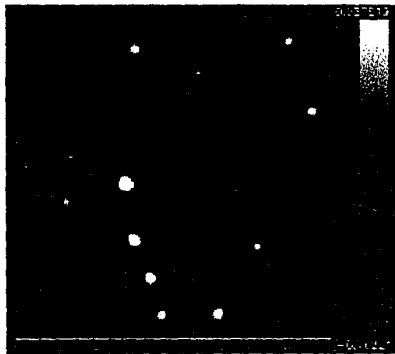
Figure 4: Observation with option 1 ( $F\lambda$  square pixels), with a final resolution of  $\lambda/2$  at  $250 \mu\text{m}$  (panels a and b), and with a final resolution of  $\lambda/4$  at  $250 \mu\text{m}$  (panels c and d)



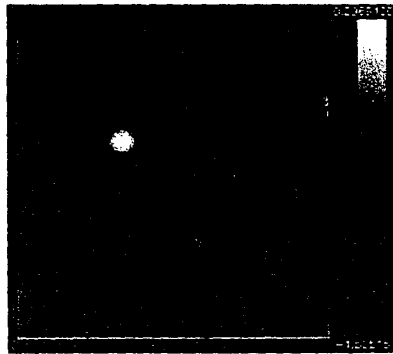
(a)  $\lambda = 250 \mu\text{m}$ , resolution of  $\lambda/2$ . Display is  $\text{Log}(f \text{ mJy/pixel})$ . Lower cut is  $1\sigma$ , upper cut is  $40 \sigma$ .



(b)  $\lambda = 500 \mu\text{m}$ , resolution of  $\lambda/4$ . Display is  $\text{Log}(f \text{ mJy/pixel})$ . Lower cut is  $1\sigma$ , upper cut is  $80 \sigma$ .



(c)  $\lambda = 250 \mu\text{m}$ , resolution of  $\lambda/4$ . Display is  $\text{Log}(f \text{ mJy/pixel})$ . Lower cut is  $1\sigma$ , upper cut is  $40 \sigma$ .



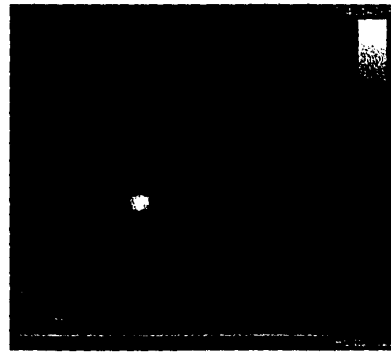
(d)  $\lambda = 500 \mu\text{m}$ , resolution of  $\lambda/8$ . Display is  $\text{Log}(f \text{ mJy/pixel})$ . Lower cut is  $1\sigma$ , upper cut is  $80 \sigma$ .

Figure 5: Observation with option 2 ( $F\lambda/2$  square pixels), with a final resolution of  $\lambda/2$  at  $250 \mu\text{m}$  (panels a and b), and with a final resolution of  $\lambda/4$  at  $250 \mu\text{m}$  (panels c and d)

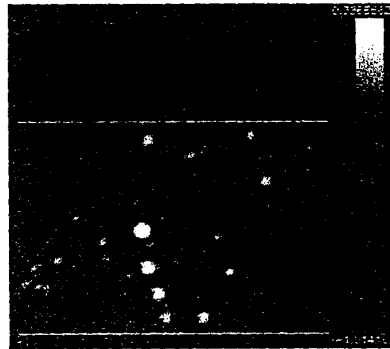




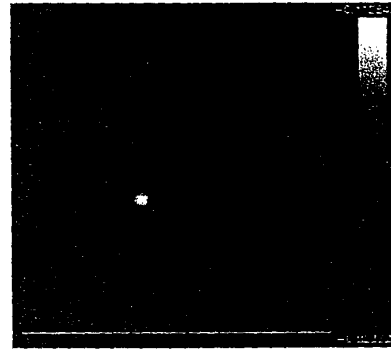
(a)  $\lambda = 250 \mu\text{m}$ , resolution of  $\lambda/2$ . Display is  $\text{Log}(f \text{ mJy/pixel})$ . Lower cut is  $10\sigma$ , upper cut is  $400 \sigma$ .



(b)  $\lambda = 500 \mu\text{m}$ , resolution of  $\lambda/4$ . Display is  $\text{Log}(f \text{ mJy/pixel})$ . Lower cut is  $10\sigma$ , upper cut is  $800 \sigma$ .



(c)  $\lambda = 250 \mu\text{m}$ , resolution of  $\lambda/4$ . Display is  $\text{Log}(f \text{ mJy/pixel})$ . Lower cut is  $10\sigma$ , upper cut is  $400 \sigma$ .



(d)  $\lambda = 500 \mu\text{m}$ , resolution of  $\lambda/8$ . Display is  $\text{Log}(f \text{ mJy/pixel})$ . Lower cut is  $10\sigma$ , upper cut is  $800 \sigma$ .

Figure 6: Observation with option 3 ( $2F\lambda$  horns), with a final resolution of  $\lambda/2$  at  $250 \mu\text{m}$  (panels a and b), and with a final resolution of  $\lambda/4$  at  $250 \mu\text{m}$  (panels c and d)

# Minutes of Splinter Session on the Scientific Requirements Document

Chairman: Walter Gear

Minutes prepared by: Matt Griffin

## General approach

It was agreed that this was appropriate. Now that the main scientific drivers are identified, quantitative numbers can be quoted, but we must be careful to avoid making reckless promises. For deep extragalactic surveys, an important requirement is to be able to detect a usefully large number of sources regardless of whether the population of high-z galaxies turns out to be at the upper or lower end of the scale consistent with credible models. This means being able to map an appropriately large area down to the confusion limit.

## Top-level requirements not mentioned in the draft

**Follow-up of Planck and SIRTf:** For follow-up using the FTS, we must make sure that the field of view is big enough given the positional accuracies that will be available. However, even with the existing 2 x 2 arcminute fov, we may be OK because (i) radio positions may be available for some objects; (ii) anything observable with the FTS can be quickly observed by the photometer or with PACS with good S/N to pin down the position.

**Co-ordinated observations with PACS:** Both galactic and extragalactic surveys will require very close coordination with PACS. At this stage, we might as well regard our top-level science requirements as extending beyond the capabilities of SPIRE. The next version of the SRD will be circulated to PACS for their information and comments and hopefully to initiate closer contacts in the future.

The relative calibration of SPIRE and PACS is very important, especially for the proper construction of SEDs spanning the two wavelength regions near the peak. Some overlap in wavelength coverage would be very useful for this. We should think about a requirement on the relative calibration of SPIRE and PACS.

## Particular points made during the discussion

1. We will need to measure the PSF very accurately in orbit, and to understand all contributions to PSF degradation (e.g., spacecraft jitter)
2. Important trade-off: In designing the photometer optics, there will be a trade-off between throughput (photon gathering efficiency) and image quality (aberrations – change in PSF shape and distortion – change in PSF size). We need the best possible angular resolution for many programmes, but what if it's at the expense of sensitivity? It is important that the design choices be based on an understanding of which is more critical for the science. This question should therefore be looked at urgently and quantified, preferably through working contacts between the Project Scientists and the optical design team.
3. It is likely that the image quality and detector performance will not be uniform across the array. Therefore it will be necessary to have observing modes which do not observe the same part of the sky with the same pixels all of the time.
4. The nominal wavelengths of the photometric bands are more or less arbitrary - anyone who thinks they should be revised should make a case.

5. FTS band overlap: we need a limit on degradation of sensitivity in the overlap region
6. Confusion is not as strong a function of angular resolution as previously thought but it is still important to
7. Chopping makes confusion worse, but to what extent is uncertain – we need simulations. But it is clear that an observing mode that does not use chopping will be significantly better for deep surveys.
8. For maximum efficiency, we should have as many detectors in the focal plane as possible regardless of whether we chop or not.
9. It is clear that the “chopper” will be required to perform complex jiggling and/or scanning motions. It is important that a specification for it be drawn up soon, which requires attention to the needs of the various observing modes and detector array options.
10. The FIRST telescope design and sharing of the focal plane are not well optimised for SPIRE. Alternatives which provide better image quality should be studied. To make progress on this we will need to quantify the potential improvements.
11. The minimum spectral resolution required for spectrophotometry with the FTS needs to be specified as it has a major impact on the sampling accuracy requirement for the mirror position.
12. Requirements on co-alignment of the arrays should be quantified.
13. For the spectrometer, enlarging the field of view would have implications for the optical design and internal layout. The beam would get larger and the off-axis image quality would be a problem. The increase in data rate would also need to be accommodated. The scientific advantages therefore need to be clarified and weighed up against the technical problems.
14. It is agreed that it would be very good to have a workshop next Spring on SPIRE science (hopefully with the participation of PACS).

## Actions

<b>AI-SRD-0056-01</b>	Send any additional comments on the draft SRD to J-P B and WKG (Dec. 18)	All
<b>AI-SRD-0056-02</b>	Produce new draft of the SRD (Dec. 31)	J-P B
<b>AI-SRD-0056-03</b>	Examine requirements derived from need to follow up Planck observations (Dec. 31)	SJO
<b>AI-SRD-0056-04</b>	Study tradeoffs between optical quality and throughput (TBD)	BMS/KD/WKG
<b>AI-SRD-0056-05</b>	Summarise the case for making SPIRE capable of observing at other wavelengths (Dec. 31)	AF
<b>AI-SRD-0056-06</b>	Organise SPIRE Science Workshop with invitation to PACS (Jan. 31)	WKG/J-P B

SJO	=	Seb Oliver
KD	=	Kjetil Dohlen
BMS	=	Bruce Swinyard
WKG	=	Walter Gear
AF	=	Alberto Franceschini
J-P B	=	Jean-Paul Baluteau

**Time sampling interferograms with an LVDT  
Oversampling and interpolation**

G.Michel  
DESPA / MEUDON OBSERVATORY

**1.1 Introduction :**

This follows a previous report [1] on the evaluation of an LVDT transducer aimed at the sampling of long wavelength interferograms. Since the sampling accuracy we are looking for might be marginal with that kind of transducer it is important trying to improve it by oversampling and interpolation.

**1.2 Experimental data available for the simulation :**

This is based on the measurements performed on a prototype drive mechanism for CASSINI / CIRS available at Meudon. The drive is servoed around a 1cm scan LVDT position transducer.

This drive mechanism system has been characterized in term of position noise with a laser interferometer. The deviation from linearity has been recorded by time sampling the position. The number of samples recorded is about 16K for the 1cm range with a scan duration of 30 sec.

This file is then used for the simulation of 4cm range LVDT after multiplication of the deviation from linearity by a factor 3.5. This is to take into account the loss in sensitivity of the transducer going from 1 cm to 4 cm .

The simulation consists in generating the synthetic interferogram of a band pass filter in the spectral range 200-300  $\mu\text{m}$  including the sampling errors. Then we evaluate the S/N in the spectrum.

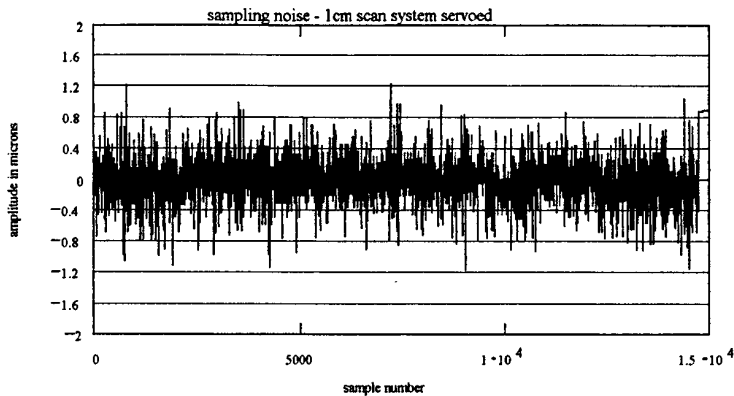


fig 1 :This is the position or jitter noise after compensation of the non-linearity. The value is  $.2 \mu\text{m rms}$  ( scan length 1cm ). The corresponding file has been used for the simulation. For a 4 cm scan this jitter figure becomes  $.2 \times 3.5 = .7 \mu\text{m rms}$  .

### 1.3 Oversampling the interferogram :

The interferogram produced is highly oversampled (factor 16) , its characteristics are :

double sided			
sample numbers	16	K	(actual 15K )
spectral band	33.3 - 50	cm-1	( 300 - 200 $\mu\text{m}$ )
absorption line	41.7	cm-1	
OPD	9.15	cm	
sampling interval	6.1	$\mu\text{m}$	
free spectral range	819	cm-1	
resolution (no apodization )	.1	cm-1	
scan duration	30	s	
modulation frequency @ 33.3 cm -1	15.2	Hz	
modulation frequency @ 50 cm-1	10.2	Hz	

To verify the oversampling effect on the S/N, we split the 16K interferogram into 8 interferograms of each 2K samples. These interferograms are FFT transformed and apodized with a simple cosine window . The results are shown in the next figures .

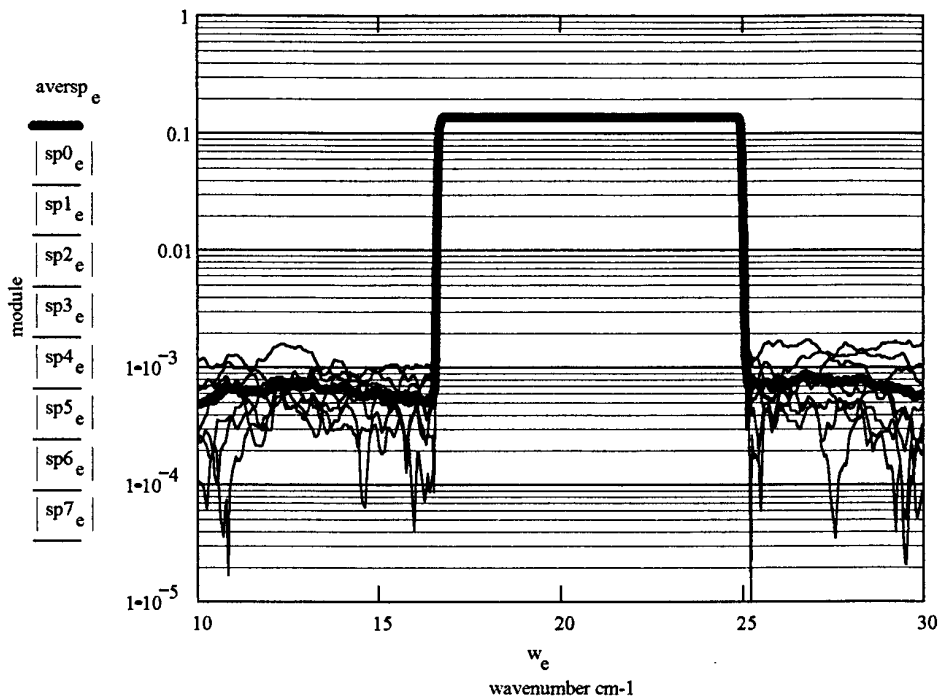


fig 2 : sp0..7 are the modules of the spectra of the 2K interferograms and aversp is the average of the 2K interferograms. The mean S/N of the spectra sp0..7 is 521 and that of the average of the 8 spectra is 992.

The oversampling by a factor 8 leads to an improvement of the S/N by 2 instead of 2.8 ( $\sqrt{8}$ ) expected. This is of course the result of a single scan. The statistic would tend to  $\sqrt{8}$  by considering multiple scans.

*For the real handling of the interferograms we will proceed to the data compression with the following steps :*

*1/ numerical filtering to extract the spectral band of interest (33-50 cm-1).*

*2/ down-sampling the interferogram ( by a factor 8 in the case of the previous simulation leading to a 2K interferogram ).*

*In that case the S/N obtained with the 2K interferogram is identical to the S/N obtained by transforming directly the original 16K interferogram.*

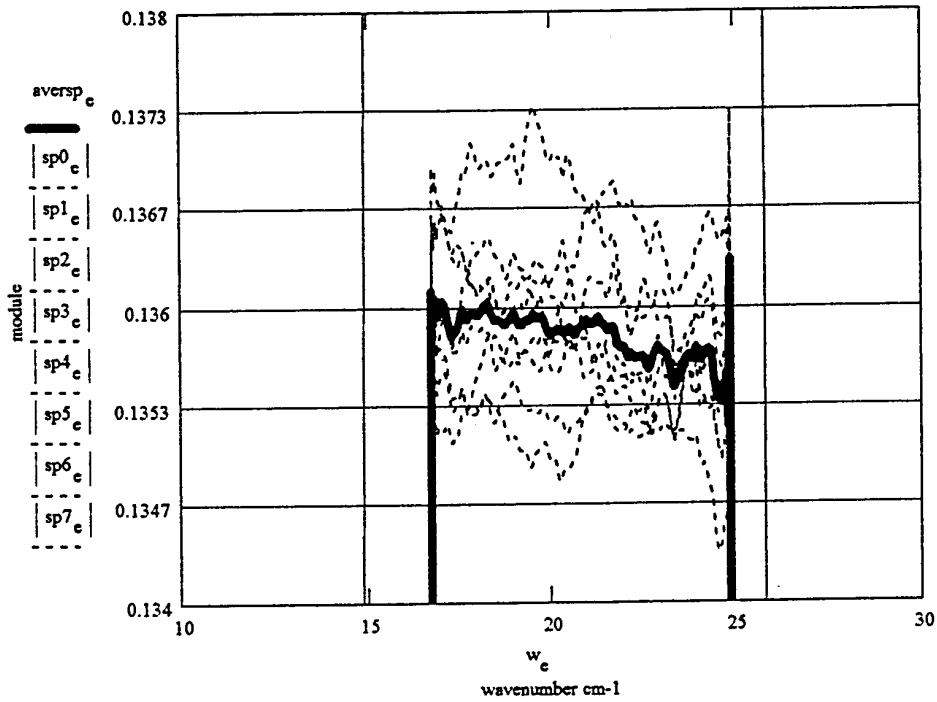


fig 3 : Same conditions as in the previous figure . The noise in the band pass is shown here with a linear scale.

As expected the oversampling improves significantly the S/N . For SPIRE the limitation will come from the data acquisition and real time processing load. At the moment a factor of 5 seems practical, leading to a potential  $\sqrt{5} = 2.2$  factor improvement of the sampling accuracy.

**The results of this simulation can be extrapolated for the different configuration of interferometer :**

Michelson Interferogram	Single Path Double Sided	Single Path Single Sided	Double Path Single Sided
Oversampling factor	16	16	16
LVDT	4cm	2cm	1cm
Resolution ( unapodized)	.1 cm-1	.1 cm-1	.1 cm-1
S/N	1000	2000	4000

#### 1.4 Improvement of the accuracy by interpolation :

Interpolation could be an additional mean of reducing the sampling error in the case we have access the position [2]. This technique is illustrated in the next figure.

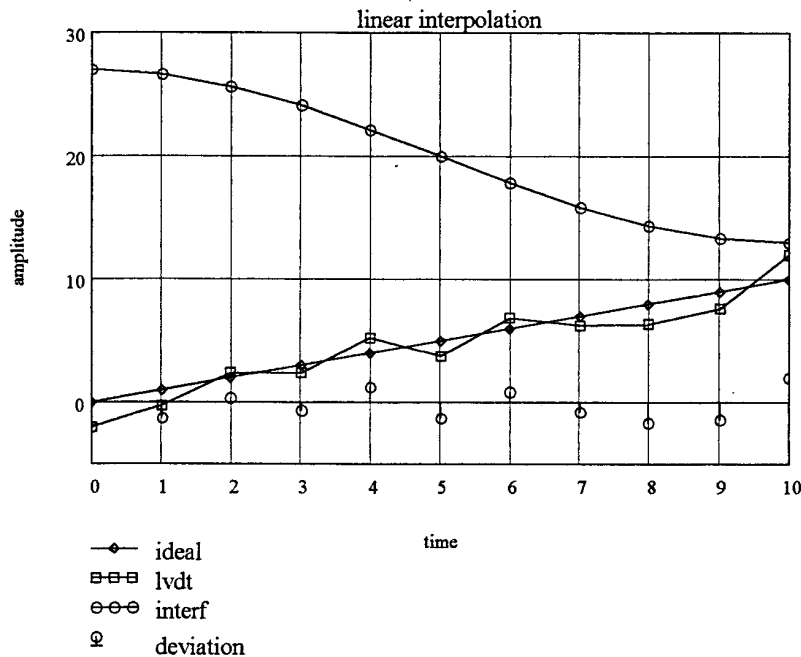


fig 4 : Principle of the interpolation. The curves shown are the interferogram, the ideal linear displacement, the lvdt actual position measurement and the deviation from ideal.

The correction consists in resampling the interferogram according to the amount of deviation from the ideal linear ramp.

To demonstrate this technique we can use the simulated interferogram and the sampling noise file and proceed to a simple linear interpolation which could be easily implemented in real time.

**At this point, it is important to note that we have here a perfect correlation between the perturbed interferogram and the sampling noise.**

**In the real case the correlation factor might be low and that kind of correction useless ( at the output of the transducer conditioner we have of course the information on the position plus electrical noise which is not related to the position ).**

Anyway what follows illustrate what we get with a correlation of 100 %. This gives an indication of the upper limit of the gain to be expected from that kind of interpolation.



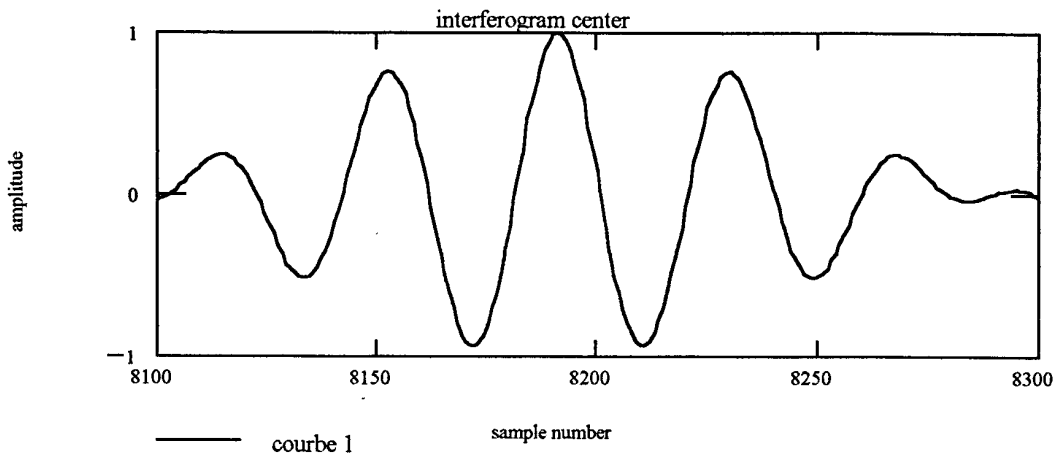


fig 5 : This is the center of the simulated interferogram including sampling errors. The error is more important at the center because since it is proportional to the derivative. This is shown in the next figure where we have the difference between the perturbed and ideal interferogram.

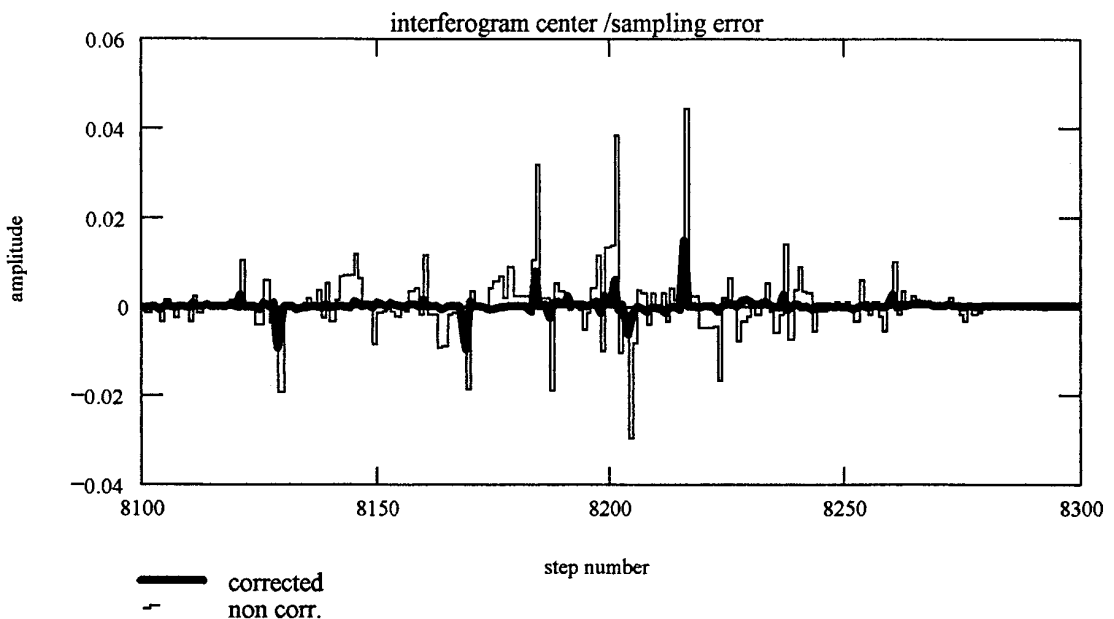


fig 6 : Here we can see the sampling errors of the non corrected and corrected interferogram. The improvement is quite significant.

Another way of showing the improvement is to compute the sampling noise over the free spectral range window.

$$wn_q := q \frac{fsr}{8192}$$

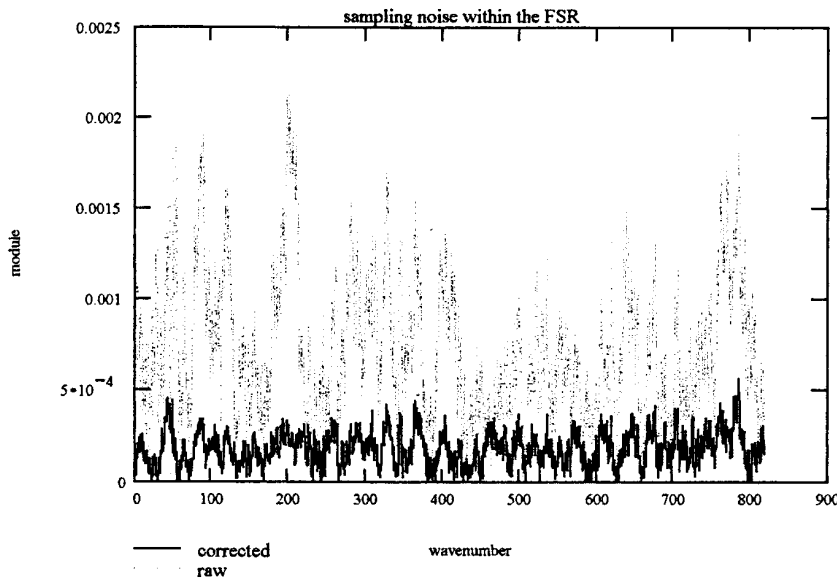


fig 7 :This shows the result of the sampling noise on the spectrum over the full spectral range with and without linear interpolation. There is a factor 4 improvement. This is the best we can get with a simple linear interpolation under the conditions of the simulation.

For the real case we can think of digitizing at the same time the interferogram and the LVDT output. It is probably equivalent to digitize the difference between the command ramp and the LVDT output i.e. the **error signal** (this will have the advantage of minimizing the dynamic range to get a good resolution with a 12 bits ADC).

The efficiency of that correction will depend on the degree of correlation between the **error signal** and the **actual jitter** as measured with the laser interferometer. To simulate this effect one can degrade the correlation index by adding white noise to the deviation from the ideal function cf (fig 4). The results are :

correlation index	S/N in the 33-50 cm-1 spectral range	gain factor corrected / non corrected
1	4108	4
.9	3045	3
.8	2451	2.4
.7	1971	1.9
.6	1600	1.5
.5	985	.9

This correlation measured on the CIRS prototype system is of the order of .4 . Under this condition the interpolation would do more harm than good.

### **1.5 Conclusion :**

As predictable, oversampling the interferogram is the very simple way of improving the sampling accuracy. As mentioned before the limitation will be the real time computation load. Altogether a factor 2 improvement over the jitter noise seems very realistic.

The interpolation can certainly be investigated on the prototype to be build. It seems that we will be strongly limited by the LVDT noise ( the part non connected to actual displacement). In presence of vibrations the situation might be different and the interpolation become more effective.

At the moment the benefit of that kind of correction seems very unlikely.

### **1.6 References :**

- [1] G.Michel The sampling of interferograms with an LVDT transducer  
Spire team meeting 15/5/98
- [2] J.C. Brasunas and G.M. Cushman  
Uniform time-sampling Fourier Transform Spectroscopy  
APPLIED OPTICS / Vol. 36, No 10 / 1 April 1997

# Minutes of Splinter Session on Detector Array Programme

Chairman: Peter Hargrave

Minutes prepared by: Peter Hargrave

Present: QMW: Peter Hargrave, Matt Griffin, Geoff Gannaway, Raul Heroso  
SAP: Jean-Louis Augueres, Louis Rodriguez, Christophe Cara  
GSFC: Juan Ramon

## 1. PROGRESS REPORTS FROM CEA/SAP AND GSFC

### SAP:-

- Results gained on detector heat capacity
- New 16x16 pixel array available mid-December for SAP tests (→QMW March)
- This array will have a range of implantation profiles on the thermometers across the array for selection of optimal implantation profile.
- Array at QMW (1 active pixel) – initial tests to be carried out before January meeting.

### GSFC:-

- Mk 1.8 array controller design complete (to control 1x8 array)
- Mechanical design for 300mK mount complete
- This mount may be used for the feedhorn option
- Mock-up 1x8 array to NIST for testing with SQUID series array in December
- NIST have completed Nyquist filter inductors
- Au/Mo TES films have been found to be very robust even when subjected to temperatures as high as 200 °C
- Mk 1.8 controller delivery (to GSFC) late December '98
- GSFC would like better definition of PDR requirements
- Written progress report has been given to Ken King

## 2. REVISIONS TO SAP TEST PLAN

- 1-pixel array at QMW
  - Optical responsivity and speed of response to be tested before January meeting
  - QMW may borrow He-3 fridge from IC if ordered fridge isn't delivered by 9/12/98
- Array (March '99 delivery) to be tested without heat-sink on readout circuit
- Thermal load to be measured in separate test
- Thermal load without 2K heatsink (i.e. to 300mK) estimated to be around 20μW.
  - Chase research fridge temp. variation of approx. 1mK/μW load.
  - Array can cope with temp. variations of around 50mK
  - Readout circuit can be operated at lower bias to compensate

## 3. ACTIONS (GSFC & JPL IN ABSENTIA)

### Reiteration of pre-existing actions:

- All array groups and QMW: Detailed interface specifications/test plans are needed for January meeting
- All array groups: Complete Bruces interface document!

**New actions:**

<b>AI-DET-0056-01</b>	Test optical responsivity & speed on SAp single pixel and present results at January Detector meeting (Jan 21)	PH
<b>AI-DET-0056-02</b>	Define interfaces between QMW/SAp for March '99 device (Jan 21)	PH/LR
<b>AI-DET-0056-03</b>	Measure heat load vs. temp. for new He-3 fridge (Jan 21)	PH
<b>AI-DET-0056-04</b>	Provide 300-mK filter dimensions to all array groups (Dec 31)	PH
<b>AI-DET-0056-05</b>	Design and build 300mK shield for March '99 device (Mar '99)	LR
<b>AI-DET-0056-06</b>	Provide staff for QMW tests (to be arranged, as needed)	SAp
<b>AI-DET-0056-07</b>	Design and build 300mK shields for other array options (to be delivered with arrays)	GSFC, JPL

# Minutes of the FTS and Optics Splinter

**Chairman: Bruce Swinyard**

**Minutes prepared by: Bruce Swinyard**

Present: A large number of people!

## **1. FTS:**

Presentations were given by Kjetil Dohlen on the analysis of the effect of noise in the mirror position measurement accuracy and by Peter Ade on the measurement of the intensity beam splitter transmission – see attached view graphs. Guy Michel submitted a report on the use of an LVDT position measurement – attached.

The major points arising from the discussion on the position measurement were:

1. The error in the position measurement has a more serious impact on the low resolution performance of the FTS.
2. Noise due to sampling errors affects the low R spectral information (photometry) much more than the high R info (line searching), especially when pt 3 is satisfied.
3. The optical filters must roll off gracefully (cosine bell or tap hat convolved with Gaussian).
4. The minimum resolution required is 20 with a goal of achieving 10.

Kjetil will redo the analysis using more realistic NEP figures and concentrating on the low-resolution performance of the instrument. There was some discussion on how the position measurement might be realised. Two ideas were proposed for further study: A tandem LVDT – or possibly a single LVDT with variable gain in the electronics - with high accuracy around the central maximum and lower accuracy at the higher frequencies; and a NIT Moire fringe readout. The implementation of both these devices will be studied further.

The intensity beam splitter appears to work with a transmission of 50% across the waveband of interest. Two will now be placed into the bench-top FTS built by Peter Ade to test the effectiveness of this device.

Guy Michel is in contact with GSFC about the implementation of the mechanism and is looking at a motor manufactured by the Swiss company ETEL.

Laurent Vigroux asked that the systems requirements for the FTS electronics and sampling be specified as soon as possible.

The next meeting will be in late January or early February to coincide with Peter completing the study into the intensity beam splitters. The location is likely to be QMW because of teaching commitments on Peter and Matt.

## 1.1 Actions:

<b>AI-FTS-0056-01</b>	Send Kjetil realistic NEP figures	BMS	4/12/98
<b>AI-FTS-0056-02</b>	Send Kjetil information on Gaussian beam optics	BMS	11/12/98
<b>AI-FTS-0056-03</b>	Recast signal to noise analysis using realistic NEP for resolution 3-20	KD	Next Meeting
<b>AI-FTS-0056-04</b>	Set date for next meeting in consultation with PARA	BMS	22/12/98
<b>AI-FTS-0056-05</b>	Study use of tandem LVDT	JPB	Next Meeting
<b>AI-FTS-0056-06</b>	Study use of NIR Moire fringe device	GM	Next Meeting
<b>AI-FTS-0056-07</b>	Provide Kjetil with sample filter profile	PARA	24/12/98

## 2. OPTICS

Kjetil reported on the outcome of his study into the issue of telescope defocus. We are sensitive to loss in detectability (Strehl ratio reduction) as the telescope – or indeed the instrument – goes out of focus. The Strehl ratio is reduced from 0.94 for a perfectly focussed system to 0.6 for a WFE of 20 microns. This raised the question of what is an acceptable loss in the Strehl ratio from all contributing factors and the distribution of the error budget through the system. No conclusion was drawn on this matter.

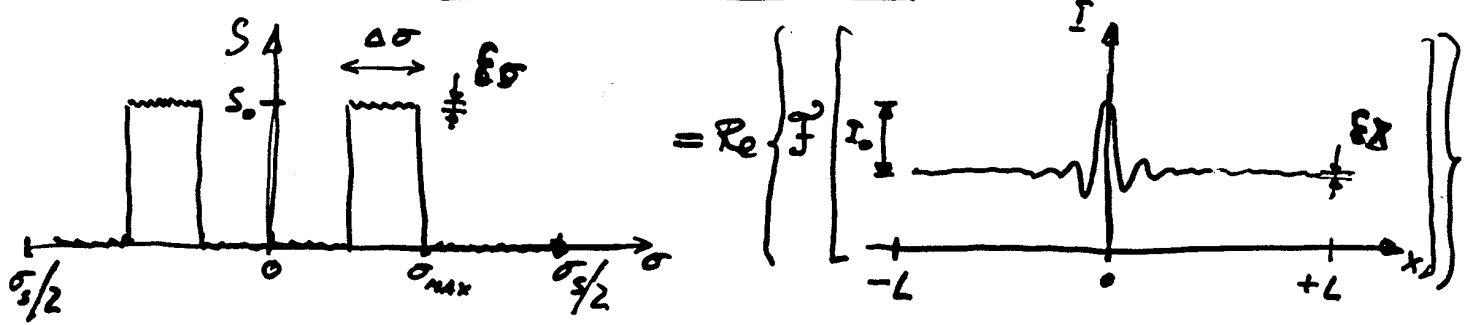
Kjetil also presented the outcome of his study into the photometer design. The pupil imaging can be improved in the current design by using a parabolic M3 – however the image quality is not good at the edges of the FOV. A new design is proposed that will cure both pupil aberration and image aberration at the expense of field distortion and an anamorphic final focal ratio. Kjetil was asked to redo the analysis of this new design with the instrument closer to the centre of the telescope FOV and using a 4x4 arc-minute FOV rather than the 5x5 in the original analysis – see note appended.

The next meeting will be contiguous with the next FTS meeting.

## 2.1 Actions:

<b>AI-OPT-0056-01</b>	Redo analysis of new photometer design with 4x4 arcmin FOV and with instrument closer to on-axis	KD	22/12/98
-----------------------	--	----	----------

FTS  
SIGNAL-TO-NOISE



$$SNR_{\sigma} = \frac{S_0}{\epsilon \sigma}$$

$$SNR_x = \frac{I_0}{\epsilon x}$$

- AREA THEOREM:  $I_0 = 2S_0 \Delta\sigma$
- PARSEVAL THEOREM:  $\int \text{noise power } d\sigma = \int \text{noise power } dx$

complex  
bracket  $\Rightarrow 2 \sigma_s \epsilon \sigma^2 = 2L \epsilon x^2$

account for  
imaginary  
part  $\uparrow$  noise  
in real  
part  $\uparrow$

$$\Rightarrow \epsilon \sigma = \epsilon x \sqrt{\frac{L}{\sigma_s}}$$

• Hence SNR:

$$SNR_{\sigma} = SNR_x \frac{1}{2\Delta\sigma} \sqrt{\frac{\sigma_s}{L}}$$

• Sampling at freq.  $\sigma_s$  represents oversampling:

$$\sigma_s = \eta \sigma_{MAX} \quad \eta \geq 2 \text{ for NYQUIST}$$

$$\rightarrow \boxed{SNR_{\sigma} = SNR_x \frac{1}{2\Delta\sigma} \sqrt{\frac{\sigma_{MAX} \eta}{L}}}$$

• Valid for any vaguely bell shaped spectrum:





# SPIRE BAND I

## SINGLE-PASS SNR

- Consider telescope background only
- Detector noise only,  $NEP = 3 \cdot 10^{-12} \text{ W}/\sqrt{\text{Hz}}$
- Assume  $\Delta\sigma = 20 \text{ cm}^{-1}$  centered @  $40 \text{ cm}^{-1} = \sigma_0$   
 $T_{\text{eff}} = 80 \text{ K}$ ,  $\epsilon_{\text{eff}} = 4\%$
- Take pixel size (square)  $\frac{\lambda_{\text{min}}}{2D}$

$$\rightarrow P = 2.3 \cdot 10^{-13} \text{ W/cm}$$

$$SNR_x = \frac{P \Delta\sigma}{NEP \sqrt{f}}$$

$$= \underline{\underline{3.4 \cdot 10^4}}$$

$$f = 20 \text{ Hz}$$

$$\begin{aligned} \text{- Hence: } SNR_\sigma &= \frac{SNR_x}{20\sigma} \sqrt{\frac{\sigma_{\text{MAX}} \eta}{L}} \\ &= \underline{\underline{2400}} \end{aligned}$$

$$\sigma_{\text{MAX}} = 50 \text{ cm}^{-1}$$

$$\eta = 2$$

$$L = 12.5 \text{ cm}$$

- Can we gain by increasing  $\eta$ ?  
→ noise spectrum?

- Co-adding increases SNR by  $\sqrt{N}$

- Need to ensure sampling error gives  $SNR_\sigma \gg 2400$

$$\rightarrow \boxed{\text{GOAL: } 10000}$$

# SAMPLING ERRORS

$$\delta I = \frac{dI}{dx} \delta x(x) \quad \delta x(x) \text{ is sampling error}$$

Bell-shaped spectrum, FWHM  $\Delta\sigma$   
centered at  $\sigma_0$

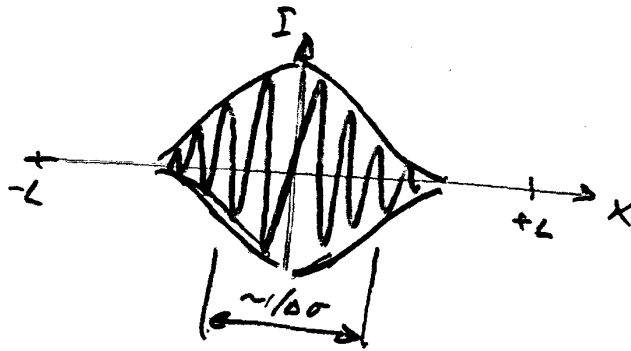
$$S = S_0 e^{-4 \ln 2 \left(\frac{\sigma - \sigma_0}{\Delta\sigma}\right)^2}$$

Interferogram: large  $\Delta\sigma$  small  $\Delta\sigma$

$$I = I_0 \cos 2\pi\sigma_0 x e^{-4 \ln 2 \left(\frac{x}{\Delta x}\right)^2}$$

where  $\Delta x = \frac{4 \ln 2}{\pi \Delta\sigma} = \frac{0.88}{\Delta\sigma} \approx \frac{1}{\Delta\sigma}$

Hence:  $\frac{dI}{dx} \approx I_0 2\pi\sigma_0 \sin 2\pi\sigma_0 x e^{-4 \ln 2 (x/\Delta\sigma)^2}$



RMS noise in interferogram:

$$\epsilon_x = I_0 \delta x \cdot 2\pi\sigma_0 \cdot \frac{1}{\sqrt{2}} \sqrt{\frac{\Delta x}{2L}} \rightarrow SNR_x = \frac{I_0}{\epsilon_x} = \frac{\sqrt{2L\Delta\sigma}}{\pi} \frac{\lambda_0}{\delta x}$$

↑ RMS of sampling error
↑ sine modulation
↑ envelope

Spectral noise:

$$SNR_\sigma = \frac{I_0}{\epsilon_\sigma} = \frac{SNR_x}{2\Delta\sigma} \sqrt{\frac{\sigma_{max}^2}{L}} = \frac{1}{2\pi} \sqrt{\frac{\sigma_{max}^2}{\Delta\sigma}} \frac{\lambda_0}{\delta x}$$

- $\sigma_{max} = 50 \text{ cm}^{-1}$
- $\eta = 4$
- $\Delta\sigma = 20 \text{ cm}^{-1}$
- $\lambda_0 = 2.50 \mu\text{m}$
- $\delta x = 0.5 \mu\text{m}$

$SNR_\sigma = 250$

$\rightarrow \frac{1}{40}$  of goal of 10 000

# IMPROVING THE SNR

• Increase oversampling  $\eta$   
 $\rightarrow \eta = 16 \Rightarrow SNR_0 = 500$

• Reduce sampling error  $5 \times$

- $\rightarrow$  Time sampling
- $\rightarrow$  Servo loop
- $\rightarrow$  Mechanical inertia

• Reduce signal level.

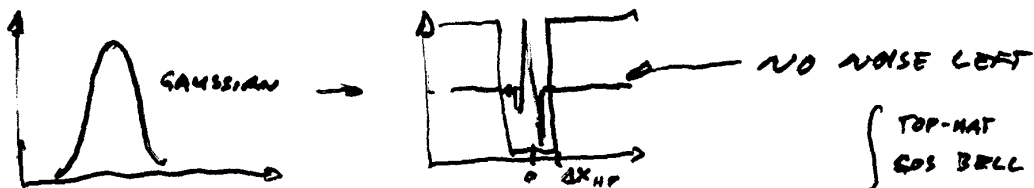
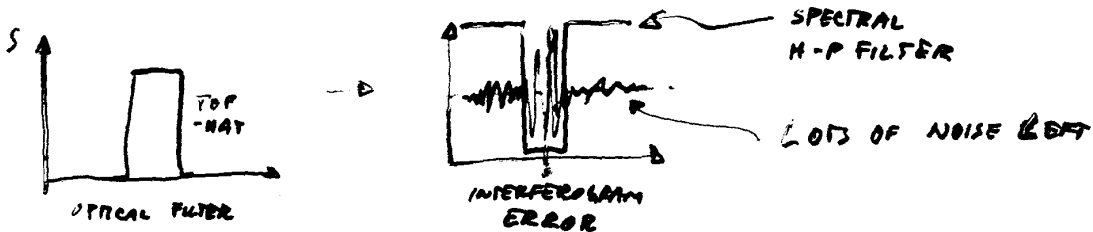
- $\rightarrow$  Reference source
- $\rightarrow$  Need:

$$\frac{I_{ref} - I_{ref}}{I_{ref}} \leq \frac{1}{40} = 2.5\%$$

$\rightarrow$  38 years: 
 $\frac{\Delta T}{T} \sim 0.5\%$   
 $\frac{\Delta \epsilon}{\epsilon} \sim 0.1$ 
  $\rightarrow \epsilon' = 44\%, T' = 75K$

• High-pass filtering of the spectrum

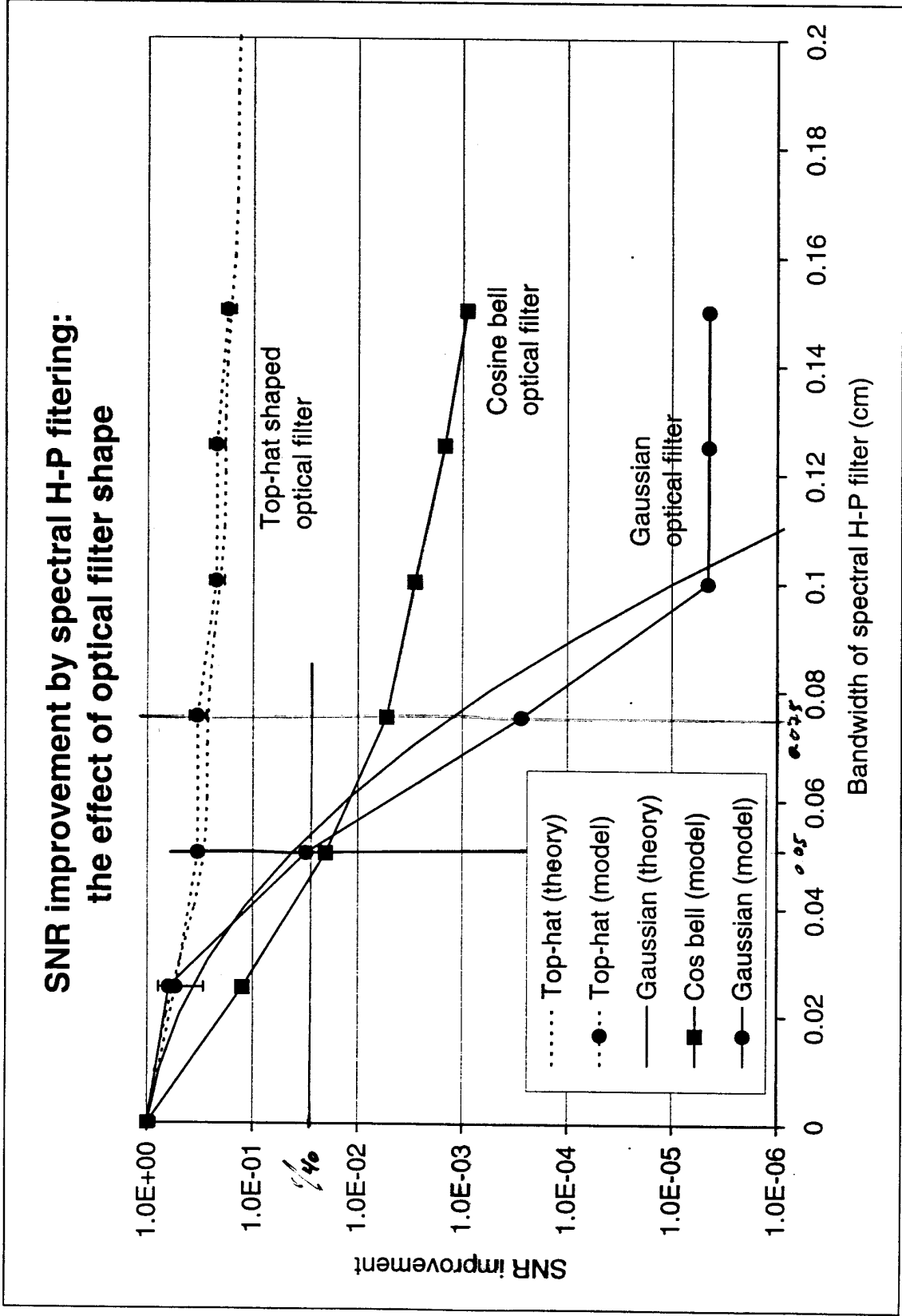
- $\rightarrow$  Loss of low R info
- $\rightarrow$  strongly dependent upon optical filter shape



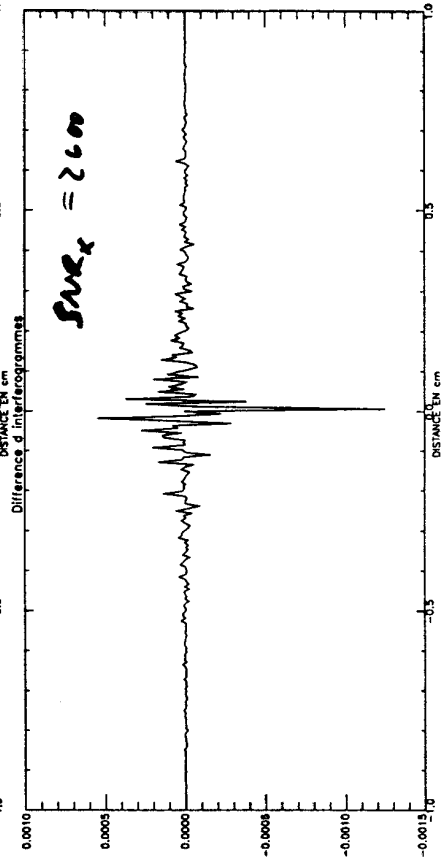
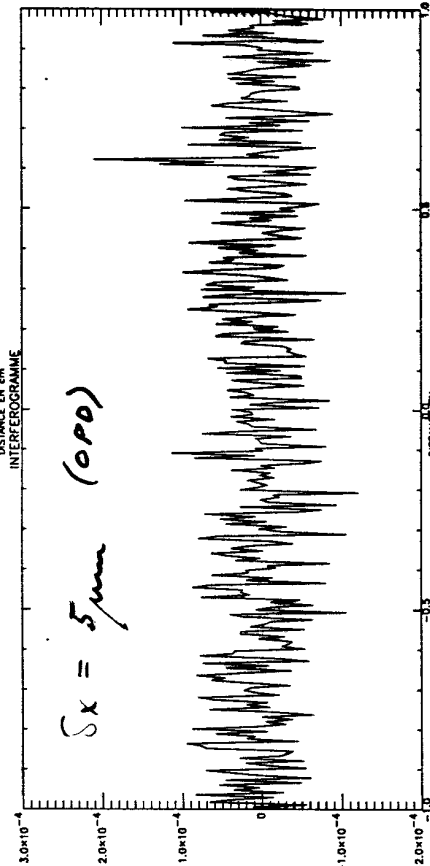
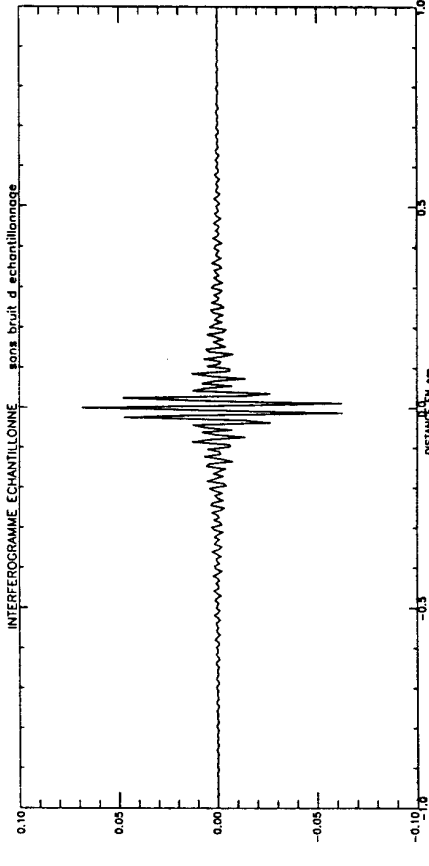
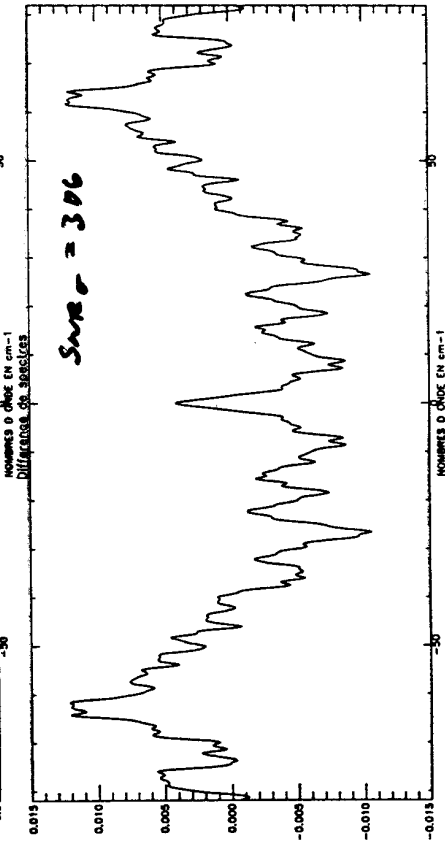
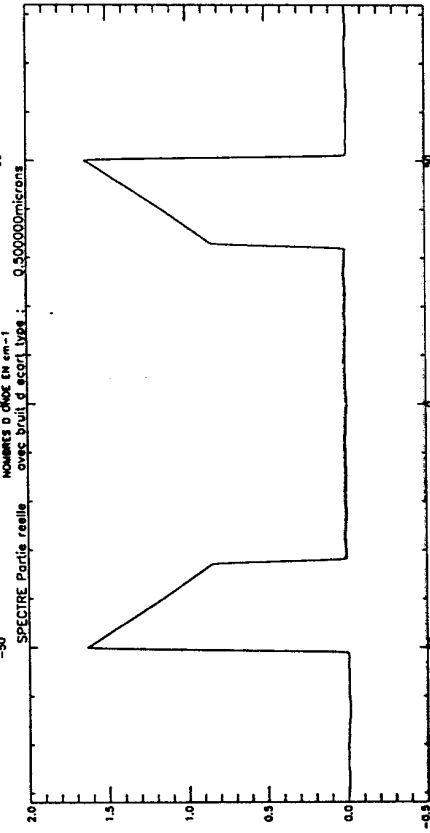
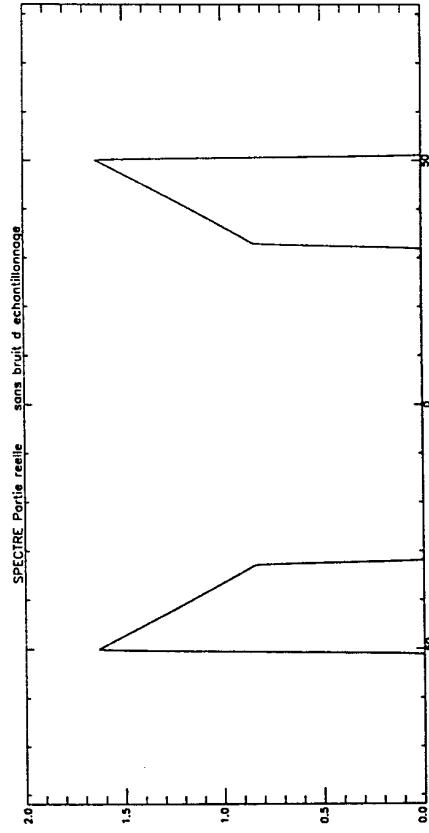
$\Delta x_{HP} = 0.075 \text{ cm} \Rightarrow 13 \text{ cm}^{-1} \Rightarrow R_{HP} = \frac{40}{13} = 3 \Rightarrow$

TOP-HAT	0.3
COS BELL	0.005
GAUSSIAN	0.0003

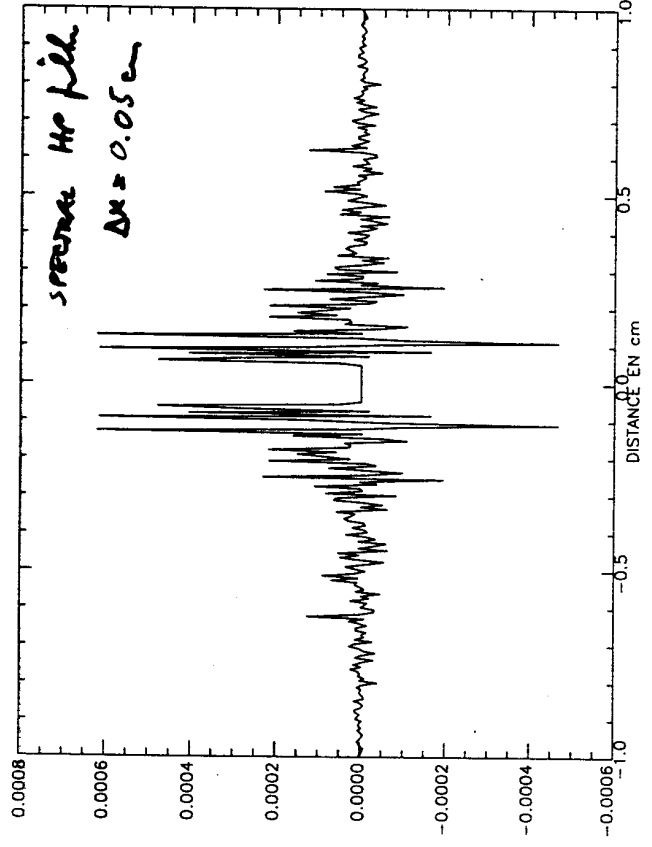
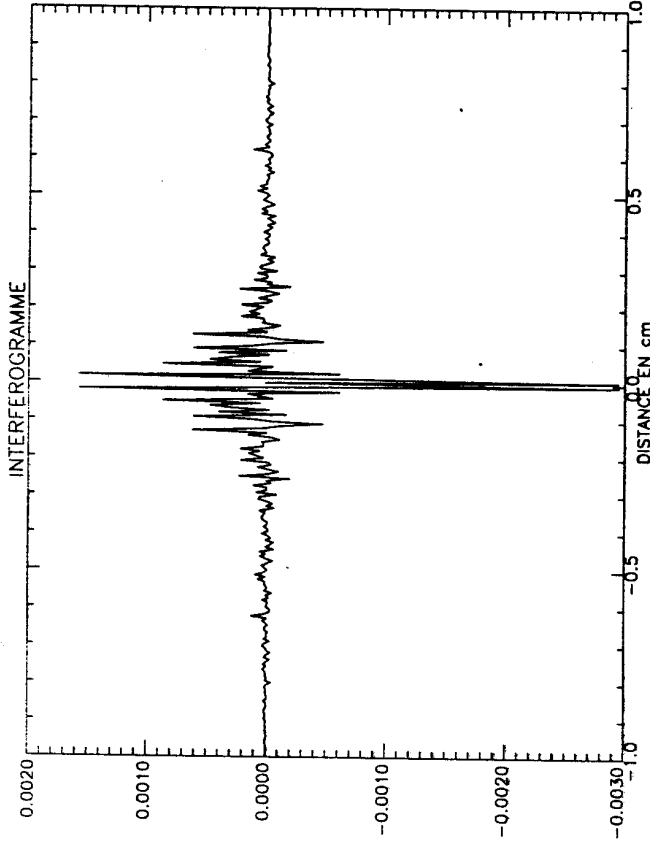
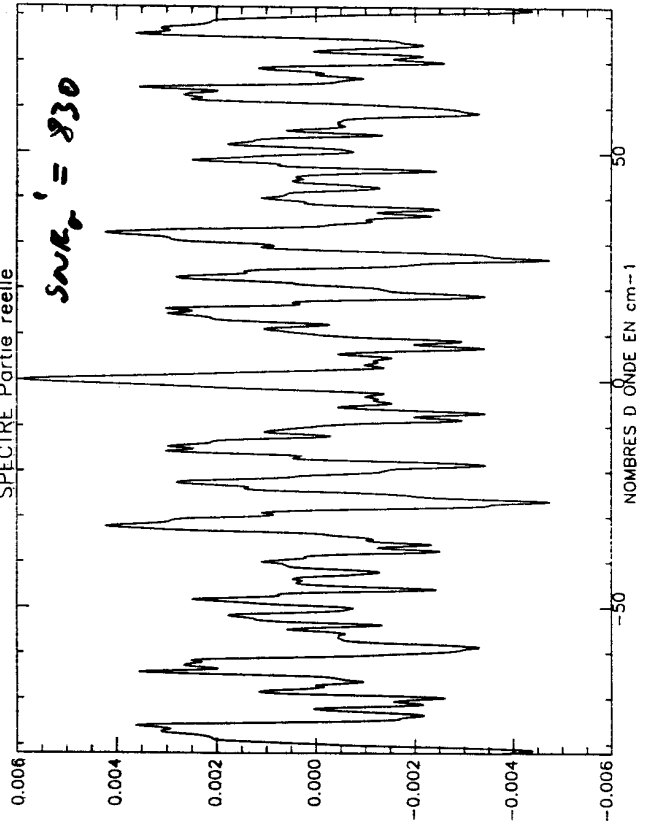
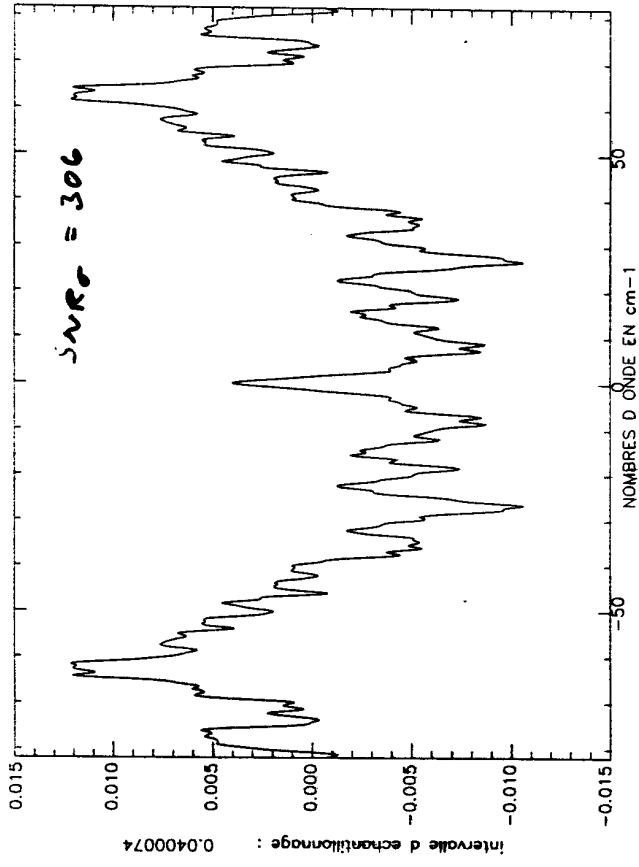
Q2 98



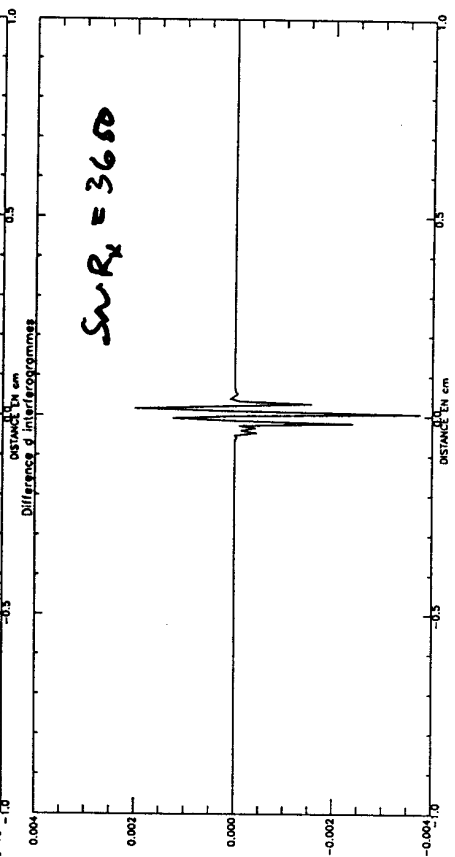
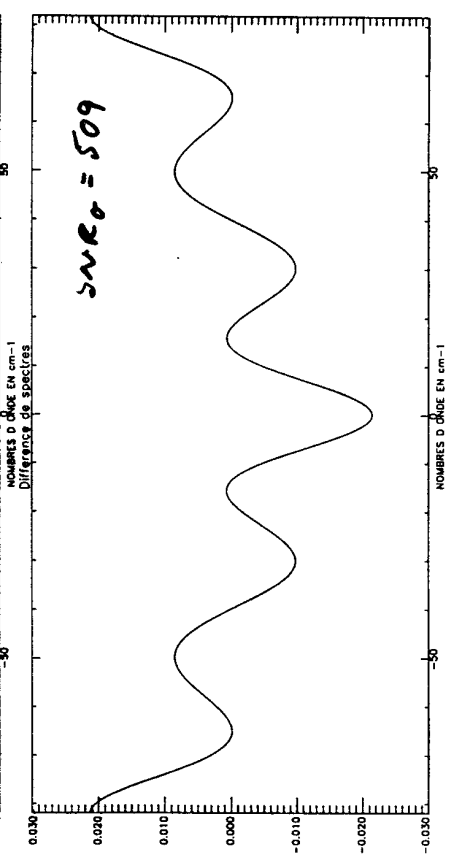
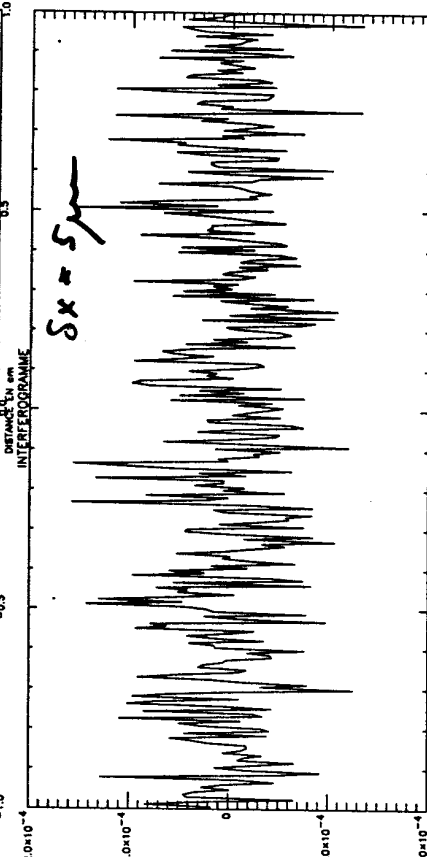
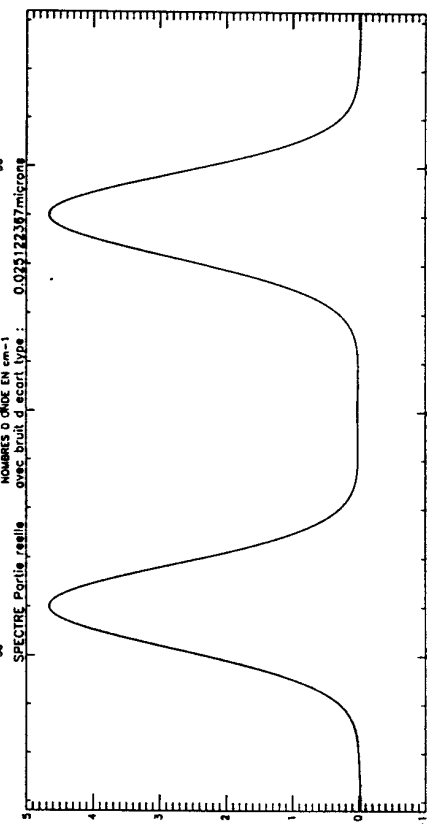
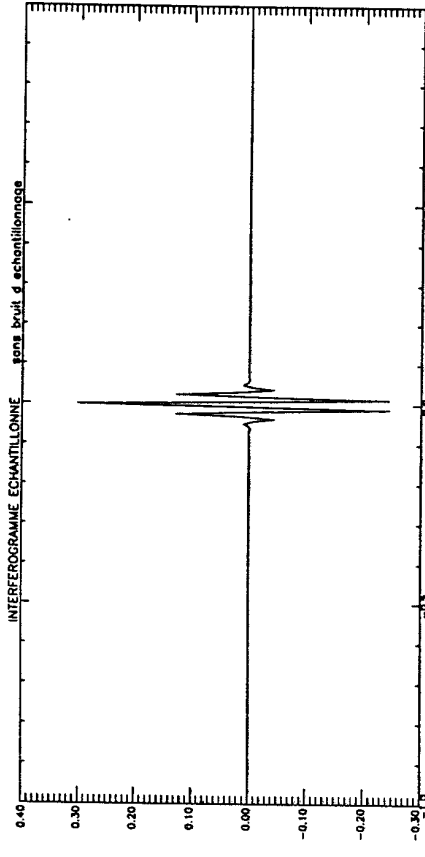
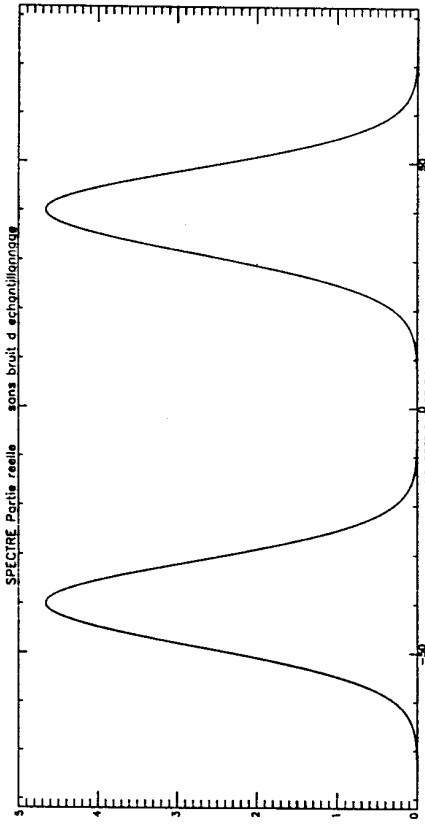
YOP-WAS OPTICAL FIBER



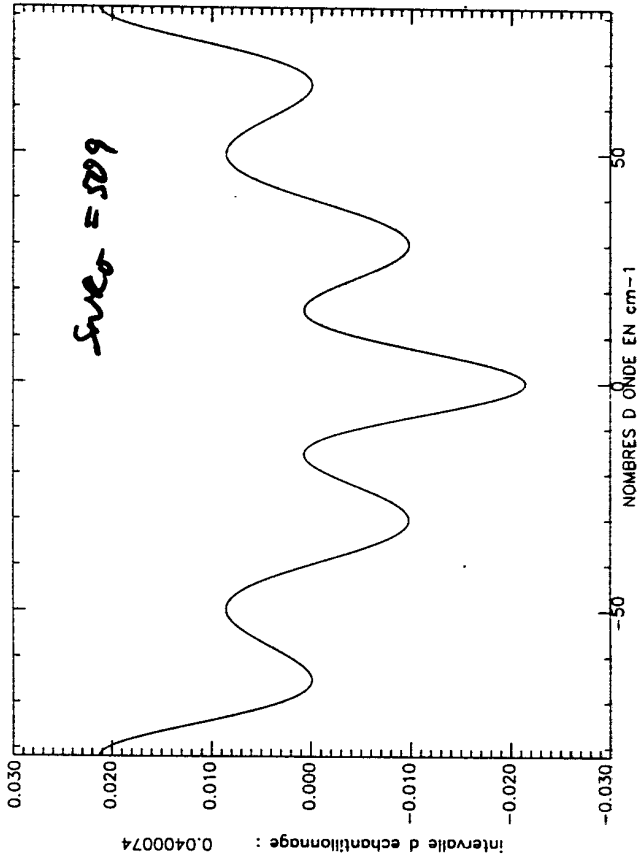
TOP-MAT OPTICAL FILTER



# GAUSSIAN OPTICAL FILTER



# GAUSSIAN OPTICAL FILTER





## FIRST-SPIRE

### New proposal for photometer optical design

Kjetil Dohlen

dohlen@observatoire.cnrs-mrs-fr

Laboratoire d'Optique, Observatoire de Marseille  
2 Place Le Verrier, 13248 Marseille Cedex 4, France

## 1. Introduction

The original photometer proposed for SPIRE is reviewed and a different design is proposed, offering improved image and pupil quality. This is achieved at the cost of surface complexity and the appearance of distortion and variable focal ratio. The overall geometry of the system up until the cold stop is largely conserved.

## 2. Design criteria

We consider here design criteria concerning optical quality. Stray-light, beam clipping, thermal aspects and mechanical implementation are not considered.

Three optical design criteria may be defined:

- 1) **Final image quality:** We assume the Marechal criterion for diffraction limited optics, i.e. Strehl ratio  $S > 0.8$  ( $S = 1$  for perfect optics). This corresponds to an RMS wavefront error at  $\lambda = 200 \mu\text{m}$  of  $w = \lambda/13 = 15 \mu\text{m}$ . An error budget must be created taking into account the theoretical image quality of the instrument, FIRST telescope quality, manufacturing and alignment tolerances, etc. This has not been done for SPIRE yet. As a reasonable target for instrument optical quality we assume  $w < \lambda/20 = 10 \mu\text{m}$ .
- 2) **Intermediate image quality:** Since the spectrometer does not work in the same plane as the photometer, it is very unlikely that aberrations present in the intermediate focal plane can be corrected by the spectrometer optics. For a diffraction limited spectrometer image, the intermediate image must therefore be better than the final image, say  $w < 8 \mu\text{m}$ .
- 3) **Pupil image quality in the cold-stop:** The cold stop avoids detectors to see anything outside the telescope pupil. If the image of the pupil onto the cold stop suffers from aberrations, the pupil image is not the same for all points in the FOV. For the cold-stop to be efficient, it must then be undersized, producing a loss of signal. Again an error budget is required to take account of all the effects affecting this performance (diffraction, alignment, etc). For the present purposes we assume a requirement for the geometrical optical design of **< 10% loss of flux at the cold stop**.

## 3. Original design

The original design (Figure 1) uses a spherical tertiary (M3) to image the FIRST pupil (M2) onto a flat chopping mirror (M4). The chopper allows the instrument FOV to be swept across the telescope focal plane. A toroidal M5 reimages the focal plane onto an intermediate image in which is located a small pick-off mirror feeding the spectrometer channel. M5 also produces an image of the pupil, located just after the flat M6. The cold stop, materializing the limiting aperture for the instrument, is located in this pupil image. A toroidal M7 relays the star-space image onto the final focal plane, providing sufficient back-focal clearance to fit two dichroics mounted at  $25^\circ$  to the beam, thus feeding three individual detector arrays.

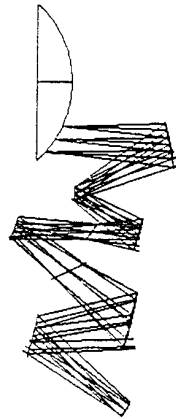


Figure 1. Present baseline design for the SPIRE photometer.

**Final image quality** is limited by the toroidal M7 which produces a nearly perfect image at the centre of the field but suffers from astigmatism at the edges (Figure 2 (a)). In the worst corner of a 5' x 5' FOV, the **wavefront error** is 32  $\mu\text{m rms}$ . The specified 10  $\mu\text{m}$  is achieved within a circle of diameter 3'.

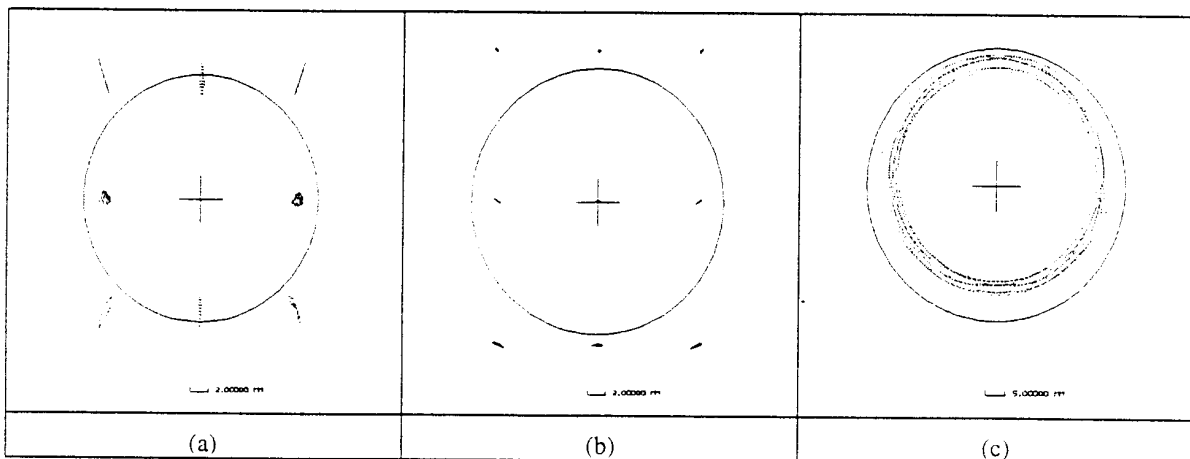


Figure 2. Raytracing results for the present baseline. (a): Final image spot diagrams for a 5' x 5' FOV. (b): Intermediate image spot diagrams. (c): Outline of the telescope pupil imaged onto the cold stop for several points in the field.

Image quality in the **intermediate focus** is within the specified 8  $\mu\text{m rms wavefront error}$  (Figure 2(b)). The image plane is tilted 35° wrt optical axis.

**Pupil imaging** suffers from coma, producing an important blurring of the image of M2 upon the cold stop (Figure 2(c)). The walk of the M2 image in the cold-stop plane is about 5 mm and the diameter of the image is about 55 mm. The cold stop must therefore be reduced to a diameter of 50 mm to avoid leakage, hence inflicting a **light loss of 17%**.

## 4. New proposal

We realized that pupil imaging was improved by changing M3 into an off-axis parabola, creating nearly optimal imaging of the telescope pupil onto M4. Adjusting the toricity of M5 slightly ensured a good pupil image also in the cold-stop plane (Figure 4(c)), achieving a **light loss due to pupil undersizing of about 8%**. A loss of final image quality was observed, however. Replacing the flat M6 and toroidal M7 by a couple of off-axis paraboloids with a collimated beam between them (Figure 3) was found to preserve the good pupil image while giving excellent quality in the final image (Figure 4(a)) with **RMS wavefront errors less than 8  $\mu\text{m}$** . The intermediate image quality (Figure 4(b)) is still sufficient but its tilt is increased to about 50°. This increase in tilt appears to be due to the use of a parabolic M3. Its impact upon image quality in the spectrometer has not been assessed.

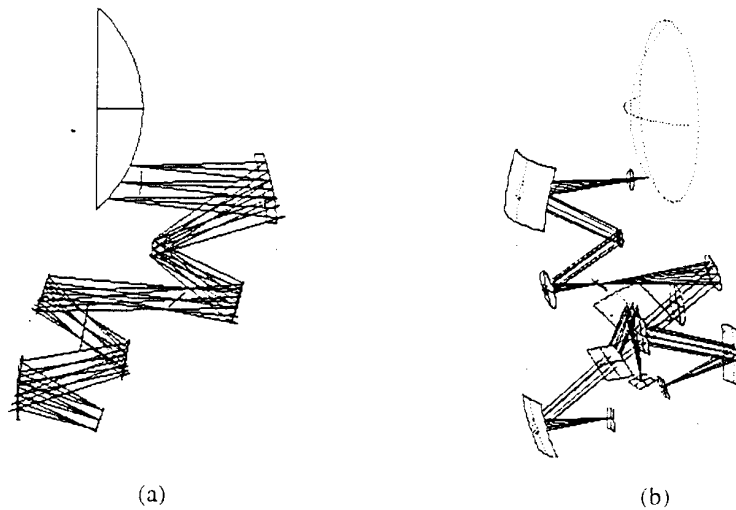


Figure 3. Proposed design for the SPIRE photometer. (a): Profile drawing with a single channel. (b): Perspective drawing with all three channels.

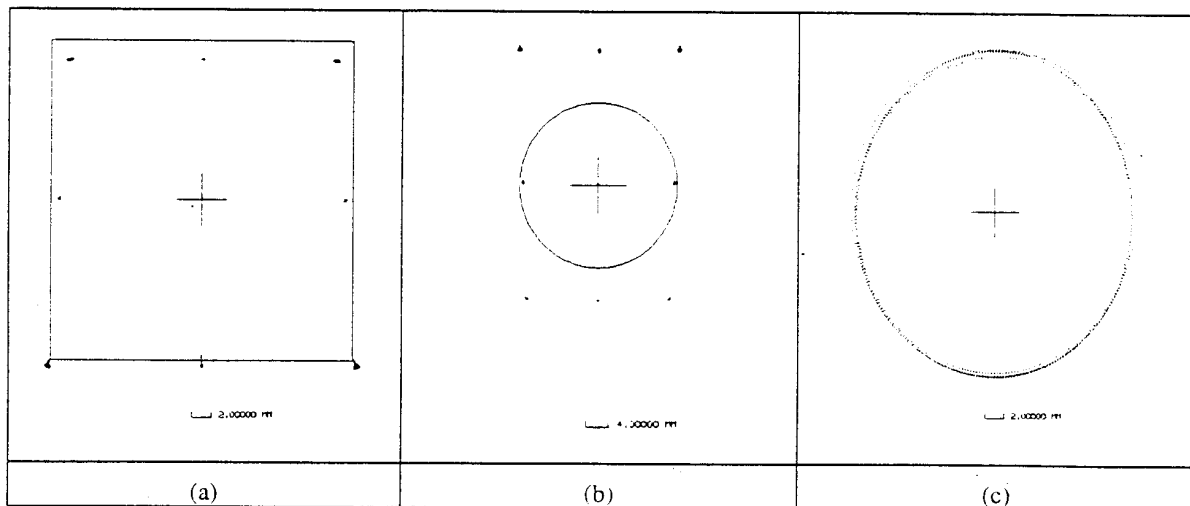


Figure 4. Raytracing results for the proposed design. (a): Final image spot diagrams for a 5' x 5' FOV. (b): Intermediate image spot diagrams. (c): Outline of the telescope pupil imaged onto the cold stop for several points in the field.

The main difference wrt the original design is that dichroics are located before rather than after M7. Each channel therefore has its own (parabolic) M7 focalizing the beam onto the detector arrays. The dichroics are mounted at  $25^\circ$  to the beam and one of them send the beam out into the plane perpendicular to the plane of the system. Figure 3(b) shows a 3D view of the complete system. The focal planes are located on three sides of an approximately rectangular box as indicated in Figure 5.

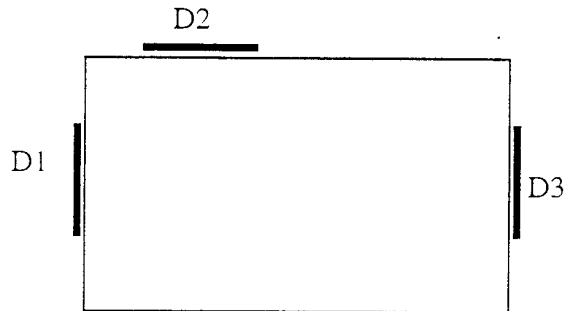


Figure 5. Arrangement of the three focal planes.

It is the use of off-axis parabolic M6 and M7 as final image relay and a cold-stop placed close to M6 which allows for the excellent image quality and the correction of the large image tilt, present in the system due to the curvature of the FIRST focal plane. The cost of this correction is a distorted image and a variable focal ratio. The distortion is illustrated in Figure 6, showing the image of a  $5' \times 5'$  object. Table 1 lists focal ratios for points A, B, and C in the FOV. Detector 1 behaves slightly better than the two others because the distance between M6 and M7 is shorter for this channel.

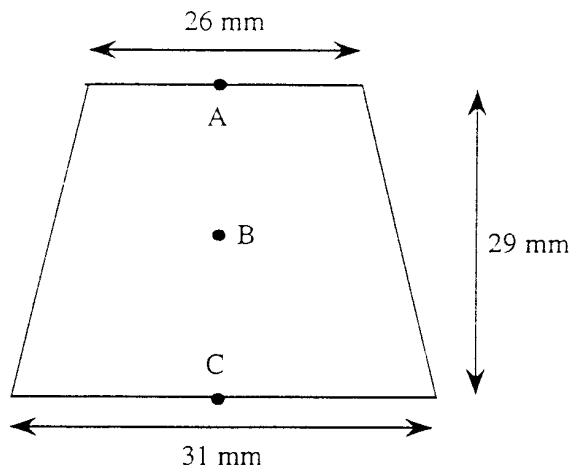


Figure 6. The image of a  $5'$  square object, illustrating the distortion of the final image. Points A, B, and C refer to Table 1.

Table 1. Tangential and sagittal focal ratios for the three points in the FOV named A, B, and C in Figure 1.

Point in FOV	Detector 1		Detectors 2 and 3	
	$F_{\text{tangential}}$	$F_{\text{sagittal}}$	$F_{\text{tangential}}$	$F_{\text{sagittal}}$
A (upper edge)	4.8	5.0	5.0	5.3
B (centre)	5.6	5.4	6.3	5.9
C (lower edge)	6.7	5.6	8.0	6.3

## 5. Conclusion

Optical design criteria and embryonic error budgets for the SPIRE photometer are presented. Comparison with the optical performance of the present baseline design indicates that it suffers from insufficient image and pupil quality. A new concept is proposed offering the required improvements. This is achieved at the cost of increased surface complexity and the introduction of distortion and variable focal ratio across the FOV. A scientific specification for the allowed variation in focal ratio is required in order to attempt a trade-off between scientific, optical, and mechanical performance.

## FIRST-SPIRE

### Impact of telescope defocus

Kjetil Dohlen

dohlen@observatoire.cnrs-mrs-fr

Laboratoire d'Optique, Observatoire de Marseille  
2 Place Le Verrier, 13248 Marseille Cedex 4, France

## 1. Introduction

ESA has requested an evaluation of the impact of telescope defocus from each of the instrument groups (meeting at ESTEC 30/9/98). Two issues should be evaluated: degradation of instrument performance and ability to measure the amount of defocus present. We treat the two questions separately, considering for the former a source barely visible above the noise, and for the latter a strong source several orders of magnitude stronger than the noise.

Telescope aberrations are represented by  $\zeta$   $\mu$ m RMS of spherical aberration, and the performance is calculated for 10, 20, and 30  $\mu$ m RMS defocus.

The analysis offered is only valid for detectors with  $\pi$  steradians field of view. It is not valid for Gaussian beams.

## 2. Performance criteria

Adding defocus or any other aberration to a system decreases the intensity of the central peak of a star image and heightens the level of the diffraction rings, finally blurring them into a halo. This outward movement of energy may be studied by calculating the point-spread function (PSF) of the system.

### 2.1 Weak source detectivity

Detectivity (D) of a weak, non-resolved stellar source may be described by the ratio of power in the PSF peak (Pp) over power in the background noise just under the peak (Pn). Since the noise level in this case is comparable to the peak of the PSF, it is much higher than the level of the diffraction rings which we may therefore ignore.

Apart from factors of proportionality we have, approximately:

$$P_p \propto W^2 S$$

and:

$$P_n \propto \sqrt{W^2} = W$$

where W is full-width at half maximum (FWHM) and S is the Strehl ratio (ratio of the actual peak PSF intensity to the theoretical, diffraction-limited peak PSF intensity). Hence, for detectivity:

$$D = P_p/P_n \propto W S \quad (1)$$

It is therefore fairly easy to determine the effect upon detectivity of small imaging perturbations. Wetherell [1, p. 303] gives the following model for Strehl ratio:

$$S \approx e^{-[2\omega w]^2 + e^2 + (2.1s)^2} \quad (2)$$

$$\text{for } \omega < 0.12, \quad e < 0.6, \quad s < 0.6, \quad \text{and } S < 0.4$$

where  $\omega$  is RMS wavefront error in units of wavelength,  $e$  is linear central obscuration ratio, and  $\sigma$  is standard deviation of the image point motion normalized to the diffraction PSF:

$$s = \sigma_m D / \lambda \quad (3)$$

where  $\sigma_m$  is standard deviation of the image point motion in angular units, D is telescope aperture diameter and  $\lambda$  is wavelength. The image point motion is modeled by:

$$I_m(r) = e^{-r^2/2\sigma_m^2} \quad (4)$$

For small wavefront errors and central obscurations, energy is moved from the central peak into the PSF wings without changing the width of the PSF peak. This is not true for image motion however, whose effect is to redistribute the energy within the central peak by widening it. The resulting FWHM may be approximated by:

$$W \approx W_0 \sqrt{1 + \left(\frac{W_m}{W_0}\right)^2} \approx W_0 \sqrt{1 + \left(\frac{2.36 \sigma_m}{I/D}\right)^2} = W_0 \sqrt{1 + (2.36 \sigma)^2} \quad (5)$$

where  $W_0$  is the unperturbed FWHM and  $W_m = 2.36 \sigma_m$  is the FWHM of the image point motion.

Detectivity as defined in Eq. 1 may then be expressed as:

$$D \propto \exp\left[-\left\{(2pw)^2 + e^2 + (2.1s)^2\right\}\right] \sqrt{1 + (2.36s)^2} \quad (6)$$

Total RMS wavefront error due to spherical aberration and defocus is given by:

$$w = (w_D)^2 + (w_S)^2$$

where  $w_D$  is RMS wavefront error due to defocus and  $w_S$  is RMS wavefront error due to spherical aberration.

The telescope primary is expected to have  $6 \mu\text{m}$  RMS of spherical aberration due to its method of fabrication. At  $200 \mu\text{m}$  this corresponds to  $w_S = 0.030$ .

The obscuration ratio of the the current FIRST telescope is  $\epsilon = 0.17$  and the image motion is  $0.3''$ , corresponding to  $\sigma \sim 0.03$  in normalized units.

With the above assumptions, Table 1 gives Strehl ratio at  $200 \mu\text{m}$  for the FIRST telescope according to Eq. 2 and detectivity according to Eq. 6. Since image motion is very small, the difference between S and D is negligible. It also shows relative detectivity given by:

$$D' = D/D(w_D = 0)$$

Table 1: Strehl ratio (S) and detectivity (D) and relative detectivity (D') as functions of RMS wavefront error due to defocus ( $w_D$ ).

$w_D$ (mm)	S at 200 mm	D at 200 mm	D' at 200 mm
0	.937	.939	1.0
10	.847	.849	.904
20	.630	.632	.673
30	.378	.379	.403

## 2.2 Defocus detection

When observing a point source much stronger than the noise with a filled focal plane array, one may detect fine changes in the PSF structure and hence, by phase retrieval, determine the amount of defocus. Calculating the PSF profile for the FIRST telescope taking into account  $6 \mu\text{m}$  RMS spherical aberration and various amounts of defocus gives an idea of the possibility of realizing such a phase retrieval.

A simple model based upon the circular symmetry of a wavefront aberrated by defocus and spherical aberration has been built. The model accounts for central obstruction but not for image motion. Figure 1 shows a comparison between the PSF for an unaberrated, unobstructed wavefront calculated at  $200 \mu\text{m}$  by the model (broken line) and the theoretical PSF calculated by the classical Airy disk formula (solid line). The difference (dotted line) is everywhere less than  $1/1000$  of the central peak and about  $1/200$  of the maximum of the first ring.

Figure 2 shows aberrated PSF profiles for  $\lambda = 200 \mu\text{m}$ . The curves are normalized to unit peak amplitude. For a signal-to-noise ratio (SRN) of 1000, one may detect changes in the second ring where effects of  $1 \mu\text{m}$  RMS defocus is clearly visible. If the SNR is of the order of 100, the detectable defocus is about  $2 \mu\text{m}$  RMS. Note that the presence of spherical aberration leaves the changes in PSF asymmetrical with respect to the best-focus position. From a single PSF image one may therefore determine not only the amount of defocus but also the direction of defocus.

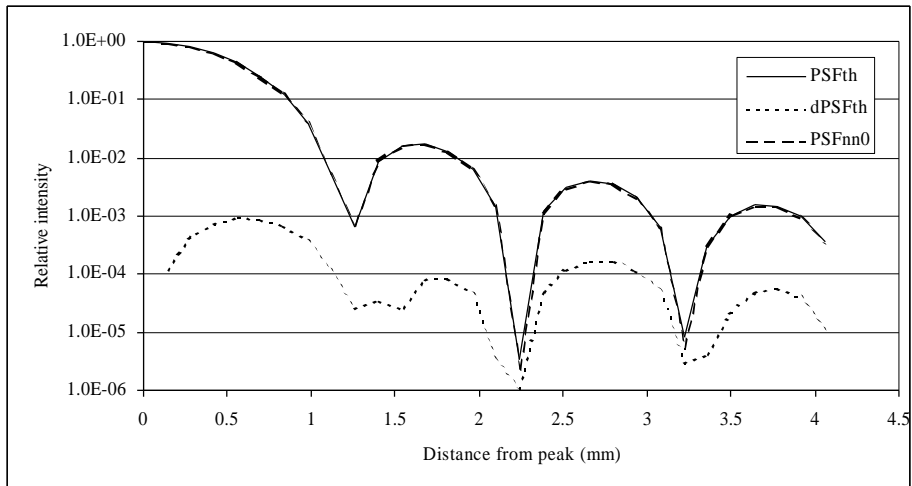


Figure 1. Verification of the model for an unaberrated, unobstructed wavefront. Theoretical PSF (solid line) compared with the modeled PSF (broken line). The dotted line shows the absolute value of the difference between the two.

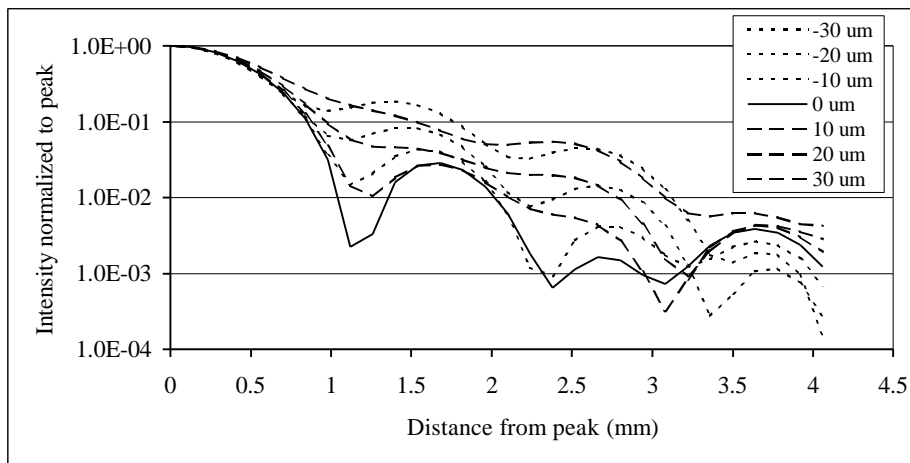


Figure 2. Normalized PSF profiles for the FIRST telescope with zero defocus (solid line) and increasing amounts of positive (broken lines) and negative (dotted lines) defocus. Defocus is given in microns of RMS wavefront error.



### 3. Conclusion

The above indicates that even at  $200\mu\text{m}$  we are quite sensitive to defocus of the FIRST telescope. Taking into account spherical aberration, central obstruction, and image motion in addition to defocus, indicates that a detectivity of 0.8 times the ideal detectivity is reached for an RMS wavefront error due to defocus of  $1\mu\text{m}$ . Letting the 0.8 criterion be relative to the detectivity of the optimally focussed telescope, the amount of defocus may be increased to  $15\mu\text{m}$  RMS. These numbers assume an ideal instrument, allowing no tolerances for aberrations in the instrument.

Modelling the PSF for a defocussed telescope indicated the possibility to detect quantitatively defocus down to  $10\text{-}20\mu\text{m}$  RMS. The presence of spherical aberration offers the possibility to estimate the direction of defocus from a single image.

### 4. References

- [1] Wetherell, W. B., "The calculation of image quality", in: *Applied Optics and Optical Engineering*, vol. VIII, Ed. R. S. Shannon, J. C. Wyant, Academic Press, London, 1980.

# Minutes of the Structure Team Splinter Meeting

Minutes prepared by: Bruce Swinyard

## Present (at least):

Wilf Oliver, Alan Smith, Colin Cunningham, Fraser Morrison, Bruce Swinyard, Kjetil Dohlen, Peter Ade.

## Summary of meeting:

Most of the meeting was spent going through the positions and masses of the optical components and explaining how everything fitted together based on existing drawings and a new summary of the mass breakdown. Wilf Oliver made annotations on the drawings and notes. Attached are two of the inputs used for this discussion - the rest are in hardcopy and will be attached to the minutes.

Some actions were then set out on how and when the structural analysis will be carried out up to Christmas. The following was agreed.

- MSSL will build a "blocks and bricks" layout in IDEAS to be reviewed with BMS on the 14th or 15th December.
- They will then wrap a structure around this and set up a reduced node model.
- MSSL will do a hand calculation of the thermal and mechanical performance of the reduced node model by Christmas.

## Actions:

<b>AI-STR-0056-01</b>	Create simplified model of SPIRE basic instrument in CAD package	MSSL	15/12/98
<b>AI-STR-0056-02</b>	Analyse performance of simplified model and verify whether the conceptual design for the instrument structure will work	MSSL	21/12/98

Logo Will Go Here	<b>SPIRE</b>	<b>Ref: SPIRE/RAL/N/nnnn</b> <b>Issue: .00</b> <b>Date: 11/12/98</b> <b>Page: 1 of 3</b>
	New Mass and Thermal Dissipation Tables	

**New mass estimate based on amalgam of Peter and Fraser's spreadsheet and new structure concept:**

First let's get the masses of what we know about – i.e. mirrors; detectors; mechanisms etc.

15-K	
M3	95
Filter	50
<b>Total 15-K hardware</b>	<b>145 x1.2 = 175</b>
4-K Photometer (common)	
Chopper	500
M5	90
filter	50
4-K Strap	300
4-K Spectrometer	
P/O Mirror	40
R1	40
R2+R3	120
R3+R4	100
R5	60
2xPolariser	100
RT1	100
Mechanism+RT2	1000 (cf GSFC 400 g for structure; LAS give <500g for LWS type motor)
C1	100
C2	60
<b>Total 4-K Hardware</b>	<b>2660 x1.2=3200</b>
2-K Photometer	
2xFilter	100
2xDichroic	100
M6	75
M7	175
M8	90
Fold 1+2	150
2-K Strap	200
3x Arrays	900
Baffles(?)	200
2-K Spectrometer	
C3	50
Polariser	50
Fold 1	60

Logo Will Go Here	<b>SPIRE</b>	<b>Ref: SPIRE/RAL/N/nmmn</b> <b>Issue: .00</b> <b>Date: 11/12/98</b> <b>Page: 2 of 3</b>
	New Mass and Thermal Dissipation Tables	

2xArrays	600
Baffles(?)	200
2-K Strap	200
2-K Cooler	
Cooler+structure	500
2-0.3 K Straps	500
<b>Total 2-K Hardware</b>	<b>4150 x1.2=4980</b>

**Table 1: “Hardware” to be supported at each temperature stage**

O.k. Now for the covers:

If we estimate the 4-K plate as being 450x550 mm and the height of the cover above it as about 180, then the surface area on the photometer and spectrometer 4-K covers will be about 6075 cm<sup>2</sup>. If we assume that they consist of 100 micron thick aluminium foil then the basic mass of each cover will be 164 g – add 20% for the stiffening structure gives 200 g for each 4-K cover. Assume the same for the 2-K cover even though it’s a bit smaller. The 15-K cover has an area of about 12000 cm<sup>2</sup> under the same assumptions it will be about 400 g.

Structure:

Take the mean thickness of the 2-K plate as being 0.5 cm (this HAS to be enough even including the optics mounts). This gives a nominal mass of 3340 g – lets take 40% margin for this as there may be some complicated bits to do with the inner enclosure and mounting of the cooler – so mass of structure “plate” is 4700 g. Take the mass of each support as 200 g – 600 g total. The total 2-K structure is then 5300 g (cf. supported hardware and covers total of 5180 g)

Again take a mean thickness of 0.5 cm for the 4-K plate; 20% margin and 1000 g for the supports – gives 5000 g for the 4-K structure.

**The total mass at 2-K is thus 10500 g**

**The total mass at 4-K is thus 8400 g**

**The total mass supported from 15-K is 19475 g** (including mirrors and filter)

With a 0.5 cm mean thickness for the base-plate; 1500 g for the support structure; 500 g for the filter support and a margin of 20% the mass of the 15-K structure is ~7000 g.

**The total mass will then be around 26.5 Kg INCLUDING 20% margin.**

Even if I’m way out on the cover masses it still looks do-able for under 30 kg.

Logo Will Go Here	<b>SPIRE</b>	<b>Ref: SPIRE/RAL/N/nnnn</b>
	New Mass and Thermal Dissipation Tables	<b>Issue: .00</b> <b>Date: 11/12/98</b> <b>Page: 3 of 3</b>

---

**Thermal Dissipation:**

The following table gives the thermal budgets for the different temperature stages for the various options and operating modes:

Logo Will Go Here	<b>SPIRE</b>	<b>Ref: SPIRE/RAL/N/ Issue: .00 Date: 11/12/98 Page: 1 of 10</b>
	<b>Possible Conceptual Layout for the SPIRE Structure</b> Author B. Swinyard	

## Introduction

As currently conceived the SPIRE structure will consist of three boxes at “15”, “4” and “2” K each supporting each other via some form of CRFP tensioned struts. The boxes themselves will also support the optics and mechanisms via structural “walls”. A preliminary analysis of this design by MSSL shows that, without going to exotic materials, it will be about 30 kg – giving a total mass for the instrument of >40 kg – this is too much.

After some discussion with various folk I propose here a new scheme for the SPIRE structure which should offer a solution to the integration of the instrument sub-systems and should, in principle, be less massive than the structural boxes. It is only conceptual and I leave the detailed engineering to those more qualified!

Also in this note I offer a first order specification for the light tightness required for each of the temperature stage covers.

## Outline Concept for the SPIRE structure.

Figures 1 and 2 show sketches of the proposed structure. The basic concept is to have a plate at 4-K (as in the present design) which is mounted from a “15-K” plate and a “15-K” support frame. The support frame needs to be massive and stiff enough to support one of the 15-K to 4-K mounts and, of course, the instrument components at 4 and 2 K. The 15 to 4-K mounts could be stainless steel tube or CRFP bipods, or, if necessary, CRFP tensioned struts as in the present concept or using the Goddard “claws” (see below). If the instrument entrance filter has to be retained in more or less its current position, then it will need to be mounted on a lightweight space frame. It is possible that this filter could be moved further down the optical path or removed completely, in this case no further structure will be required except that to hold the thermal cover (more on this later).

The optics and mechanism for the FTS are mounted directly on one side of the 4-K plate and the chopper and the 4-K optics for the photometer are mounted on the other side. Another plate, to be cooled to 2-K, is mounted off the 4-K plate again using CRFP or stainless steel tube construction bipods in a three-point mount configuration. If the thermal budget and mechanical constraints are such to prevent the use of bipods then a system similar to that used by Goddard for the detector mounts might be used with “claws” and CFRP tensioned struts or, in extremis, Kevlar string. Figure 3 shows a possible arrangement for the “claw” with CRFP struts. This 2-K plate will hold the majority of the optics for the photometer and could be used to mount the detectors and the <sup>3</sup>He cooler. However, the straylight constraints on the cover of the 2-K box will be severe (see below) and it maybe advantageous both from a structural and a straylight point of view to mount the detectors and their attendant sub-systems in a separate enclosure.

There will be lightweight but light-tight covers mounted over the 2-K plate, each side of the 4-K plate and a light-tight thermal shield over the whole instrument attached to the 15-K structure. At certain strategic points it may be that walls machined from the solid plates will have to be used to absolutely guarantee the integrity of the straylight control – this is discussed further below.

An analysis by LAS has shown that the alignment tolerances for the mirrors, on the photometer at least, can be met by standard machining techniques (*e-mailed Kjetil/Dominique to confirm actual number*). A possible concept for how the optical elements might be mounted from the structure is shown in figure 4. Here the mirror is of the same general type as used on the LWS with a central threaded stalk machined into the rear surface. The rear surface of the mirror and the contact surface

Logo Will Go Here	<b>SPIRE</b>	<b>Ref: SPIRE/RAL/N/ Issue: .00 Date: 11/12/98 Page: 2 of 10</b>
	<b>Possible Conceptual Layout for the SPIRE Structure</b> Author B. Swinyard	

of the mirror mount are accurately machined so that when the mirror is attached via a nut on the stalk, the mirror is aligned with no further adjustment. The basic form of the mirror mount is a frustum machined from the solid plate and with as much material removed as possible.

### Requirements on the covers

Figure 5 illustrates the essential elements of the straylight control strategy for the SPIRE instrument. At each temperature stage there is a cover which is designed to intercept the radiation from the previous temperature stage, thus limiting the stray power on the detector to a small fraction of that coming from the telescope via the optical train. This last is of the order of a few pW – the input power from the 30-K shield is of the order of a few mW (see below); the attenuation required is therefore of order  $10^{-9}$  – an extremely challenging prospect! However, not every shield has to have this level of attenuation because each shield is also radiating power onto the next. One criterion we could adopt is that the attenuation of a given shield should be such as limit the radiation from shield at the next highest temperature to no more than 1% of the radiation from the shield itself, or other “legitimate” sources of background radiation.

Adopting this method, the radiation falling on the outside of the instrument, the 15-K shield, from the 30-K cryostat shield is:

$$Q_{30-15} = \epsilon_{30}\sigma T_{30}^4$$

This is not the absorbed power, but an estimate of the actual level of radiation. It doesn't make much difference but this is more pessimistic. Adopting  $\epsilon \sim 0.2$  for all surfaces (again a pessimistic value) the power falling on the 15-K shield is  $\sim 9.2 \text{ mW/m}^2$ . The surface area of the 15-K shield is about  $1.2 \text{ m}^2$  so the total power is  $\sim 11 \text{ mW}$ .

Similarly the power from the 15-K shield falling on the 4-K shield is about  $0.57 \text{ mW/m}^2$  and the area of each of the 4-K shields is about  $0.5 \text{ m}^2$ :  $1 \text{ m}^2$  total. If the 15-K shield is to attenuate the power from the 30-K shield to 1% of this value then the attenuation required is:

$$A_{15} = \frac{0.57 \times 0.01}{11} = 5.2 \times 10^{-4}$$

To illustrate what this means, it is the equivalent of a  $5.2 \times 10^{-4} \times 1.2 \times 10^6 = 621 \text{ mm}^2$  hole in the 15-K cover – a hole of 28-mm diameter. If the temperature of the outer cover turns out to be lower, 9 K say, then the equivalent hole is one of 10-mm diameter or  $81 \text{ mm}^2$ . So, to allow for some margin in the temperature of the outer cover, the integrated area of all the holes through the outer cover must be no more than  $81 \text{ mm}^2$  and the attenuation must be  $6.7 \times 10^{-5}$ .

The radiation from the 4-K shield falling on the 2-K shield will be  $2.9 \mu\text{W/m}^2$ . If we assume that the area of the 2-K cover is also  $0.5 \text{ m}^2$  then the total radiated power is  $\sim 1.5 \mu\text{W}$ . Then attenuation required for the 4-K cover is then given by:

$$A_4 = \frac{0.0015 \times 0.01}{0.57} = 2.6 \times 10^{-5}$$

Logo Will Go Here	<b>SPIRE</b>	<b>Ref: SPIRE/RAL/N/ Issue: .00 Date: 11/12/98 Page: 3 of 10</b>
	<b>Possible Conceptual Layout for the SPIRE Structure</b> Author B. Swinyard	

This is equivalent to a 13-mm<sup>2</sup> – 4-mm diameter - hole in the 0.5-m<sup>2</sup> 4-K cover. If the temperature of the outer cover is lower than 15 K then this criterion becomes more relaxed – however we should adopt pessimistic values at this stage.

To calculate the attenuation required for the 2-K cover we must now use the predicted background power falling on the detectors for the comparison. Taking an average value of 7 pW for all bands and keeping the 1-% limit we get an attenuation of:

$$A_2 = \frac{7 \times 10^{-6} \times 0.01}{1.5} = 4.7 \times 10^{-8}$$

Equivalent to a 0.023 mm<sup>2</sup> - 0.17 mm diameter - hole in the 0.5-m<sup>2</sup> 2-K cover. This will be a very difficult specification to meet. Even limiting ourselves to 10% of the background power means having an integrated pinhole specification of 0.23 mm<sup>2</sup> – a 0.5-mm diameter hole. To achieve anything like this level means that we will probably have to have walls in the 2-K enclosure surrounding the detectors that are machined from the solid and exceptionally tight fitting lids; again these will probably have to be solid aluminium. The problem is compounded by the need to have wiring and, possibly, thermal straps piercing the 2-K enclosure. Figure 6 illustrates how the covers for the photometer might be arranged. At this level of straylight control we are going to have to do some detailed calculation of the straylight environment using APART.

### Summary and other points

Table 1 summarises the results of this first order cover specification and gives recommendations for the materials and surface finish for each of the covers.

The figures for the thermal input from the structural supports given in the IID-B viz. 138 μW for 15-4 K and 4.5 μW from 4-2 K are very low. The figures for the power onto the 4-K and 2-K stages given to ESA were 7.3 mW and 2.5 mW respectively. Therefore we should entertain more conservative engineering solutions for the supports, such as thin walled stainless steel tubes, which will reduce the level of risk in the programme whilst increasing the thermal load owing to the support conductance.



Logo Will Go Here	<b>SPIRE</b>	<b>Ref: SPIRE/RAL/N/ Issue: .00 Date: 11/12/98 Page: 4 of 10</b>
	<b>Possible Conceptual Layout for the SPIRE Structure</b> Author B. Swinyard	

Cover	Assumed Area	Attenuation Requirement	Equivalent Integrated Pinhole Area	Suggested material/construction	Surface Finish
15-K	1.2 m <sup>2</sup>	7x10 <sup>-5</sup>	80 mm <sup>2</sup>	Metal (copper?) foil over lightweight frame	Inner and outer shiny
4-K	2 x 0.5 m <sup>2</sup>	2x10 <sup>-5</sup>	13 mm <sup>2</sup>	GFRP or CRFP with metal foil covering	Inner and outer shiny: some regions to be blackened as identified by APART model
2-K (outer)	0.5 m <sup>2</sup>	At least: 5x10 <sup>-7</sup> Goal is: 5x10 <sup>-8</sup>	0.2 mm <sup>2</sup> 0.02 mm <sup>2</sup>	GRFP or CRFP with metal foil covering	Outer shiny with some parts blackened as identified by APART model. Inner black
2-K (inner)	N/A	See caption	See caption	Integral aluminium wall with aluminium lid	Inner and outer black

**Table 1: Summary of specifications for SPIRE instrument covers. Figures for the 2-K (outer) refer to the outer and inner taken together.**

Logo Will Go Here	<b>SPIRE</b>	<b>Ref: SPIRE/RAL/N/ Issue: .00 Date: 11/12/98 Page: 5 of 10</b>
	<b>Possible Conceptual Layout for the SPIRE Structure</b> Author B. Swinyard	

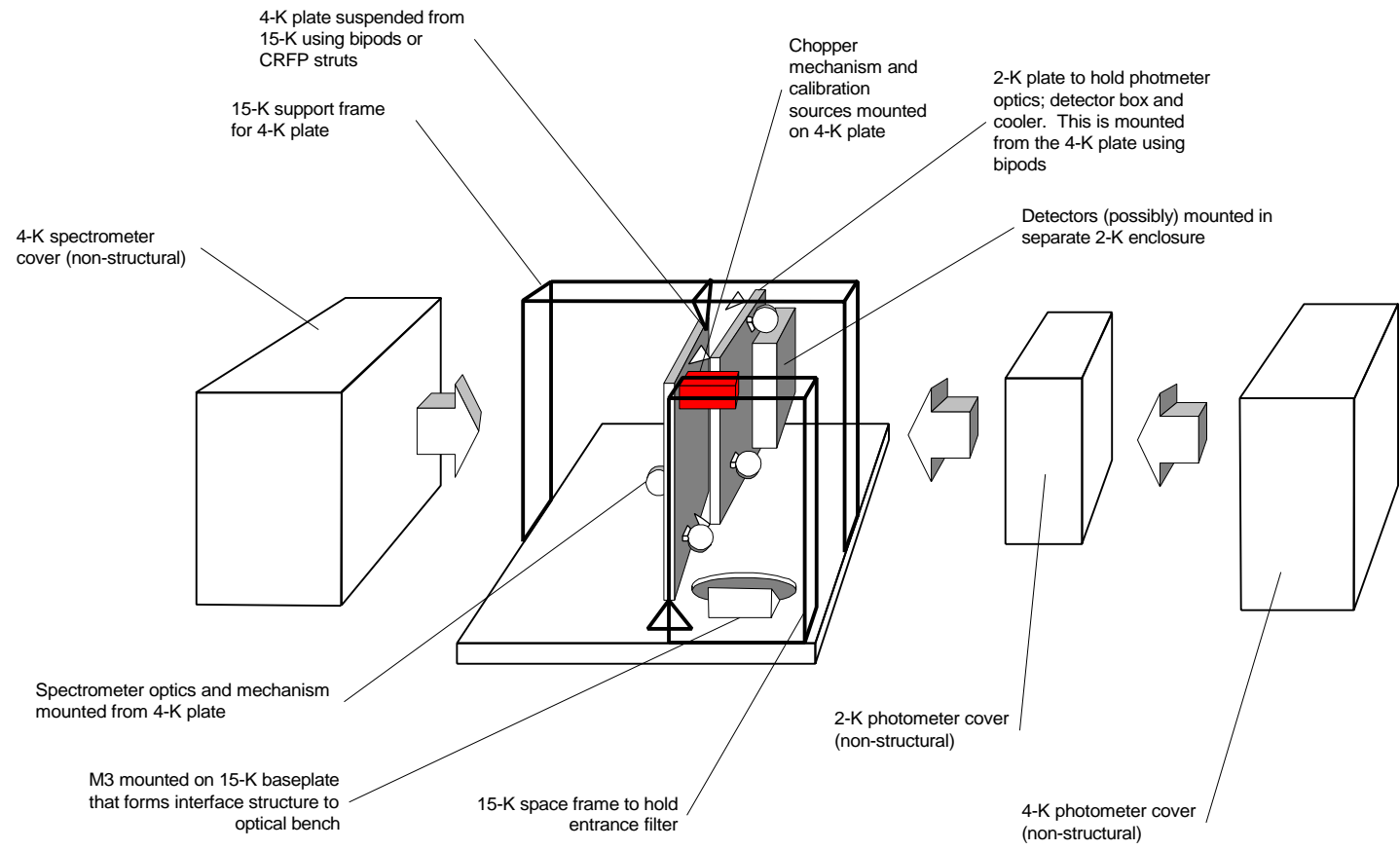


**Figure 1: Conceptual layout for the SPIRE structure based on non structural covers (15-K cover not shown)**

Logo Will Go Here	<b>SPIRE</b>	<b>Ref: SPIRE/RAL/N/</b> <b>Issue: .00</b> <b>Date: 11/12/98</b> <b>Page: 6 of 10</b>
	<b>Possible Conceptual Layout for the SPIRE Structure</b> Author B. Swinyard	

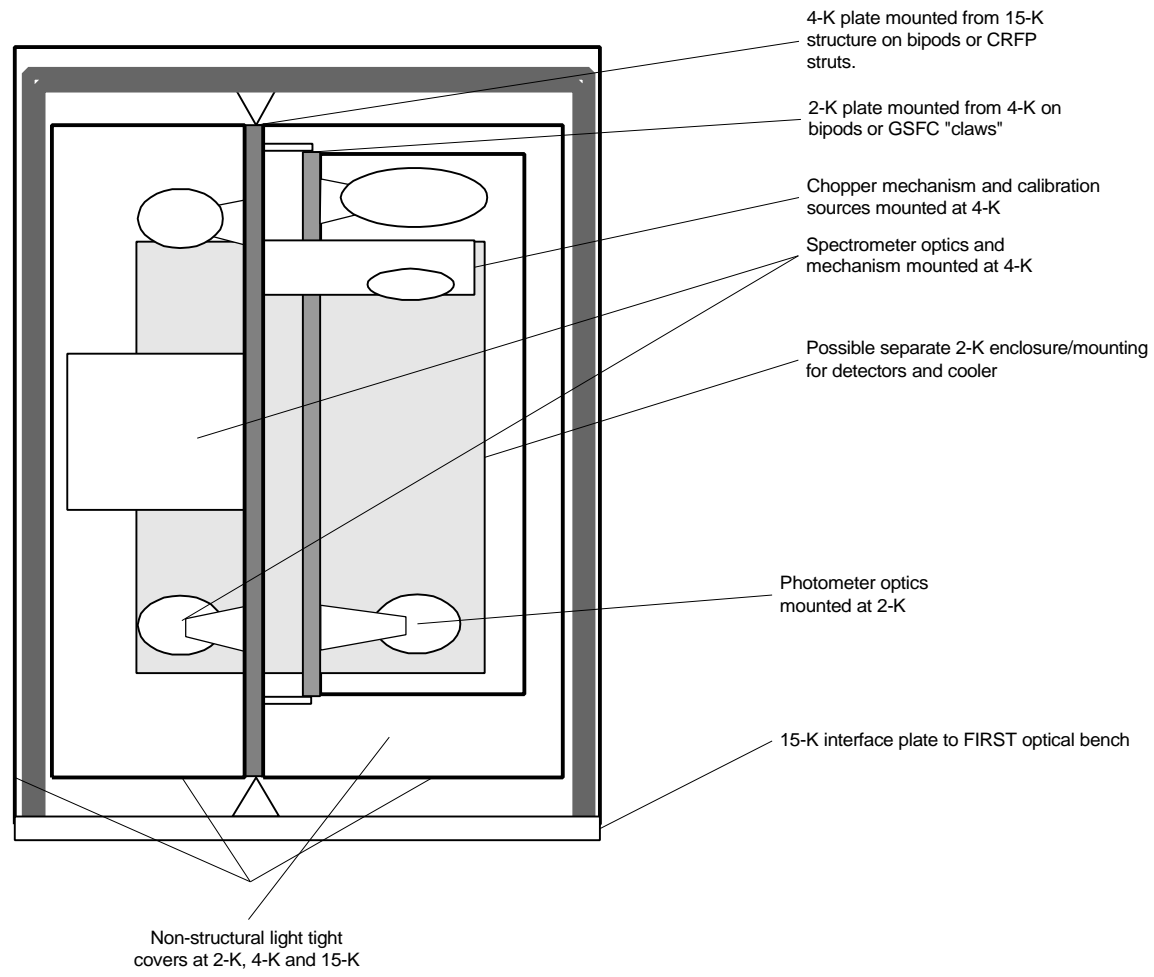


**Figure 2: End on view of conceptual layout for SPIRE structure**

Logo Will Go Here	<b>SPIRE</b>	<b>Ref:</b> SPIRE/RAL/N/ <b>Issue:</b> .00 <b>Date:</b> 11/12/98 <b>Page:</b> 7 of 10
	<b>Possible Conceptual Layout for the SPIRE Structure</b> Author B. Swinyard	

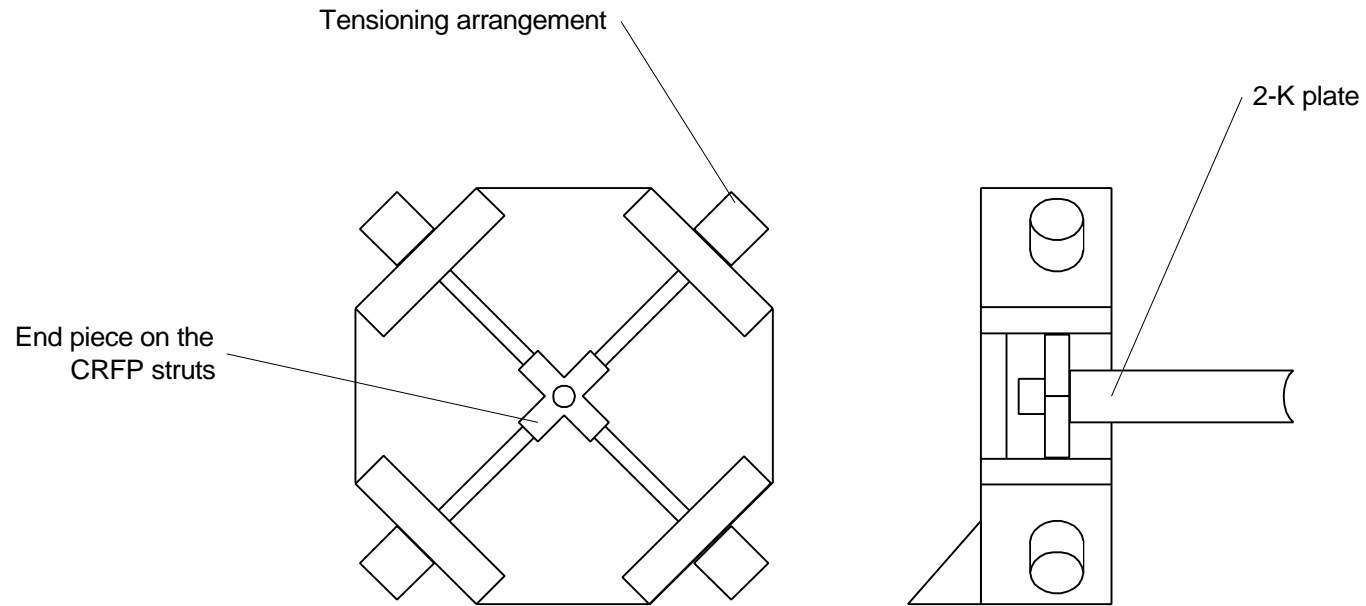


**Figure 3: Possible mounting for 2-K plate a la GSFC**

Logo Will Go Here	<b>SPIRE</b>	<b>Ref: SPIRE/RAL/N/ Issue: .00 Date: 11/12/98 Page: 8 of 10</b>
	<b>Possible Conceptual Layout for the SPIRE Structure</b> Author B. Swinyard	

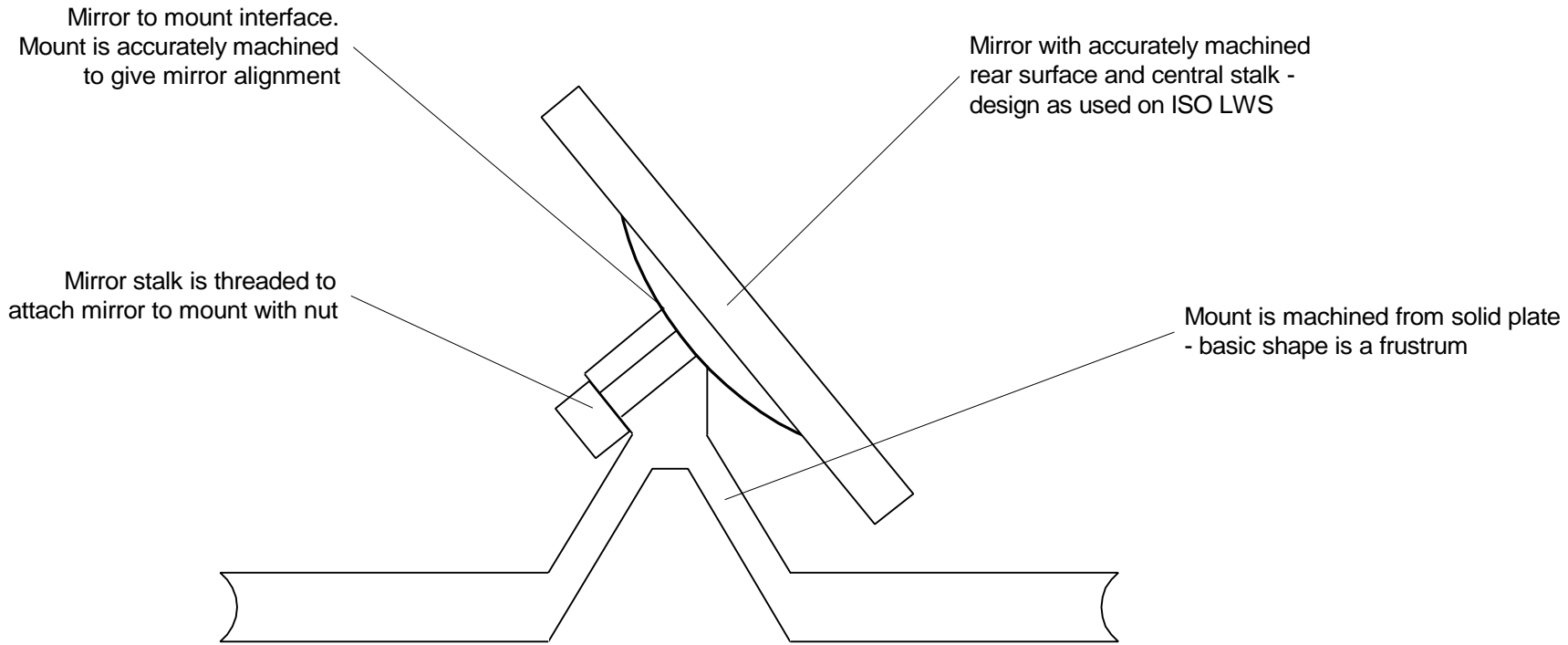


**Figure 4: Concept for mounting mirrors on 4-K and 2-K plates**

Logo Will Go Here	<b>SPIRE</b>	<b>Ref: SPIRE/RAL/N/</b> <b>Issue: .00</b> <b>Date: 11/12/98</b> <b>Page: 9 of 10</b>
	<b>Possible Conceptual Layout for the SPIRE Structure</b> Author B. Swinyard	

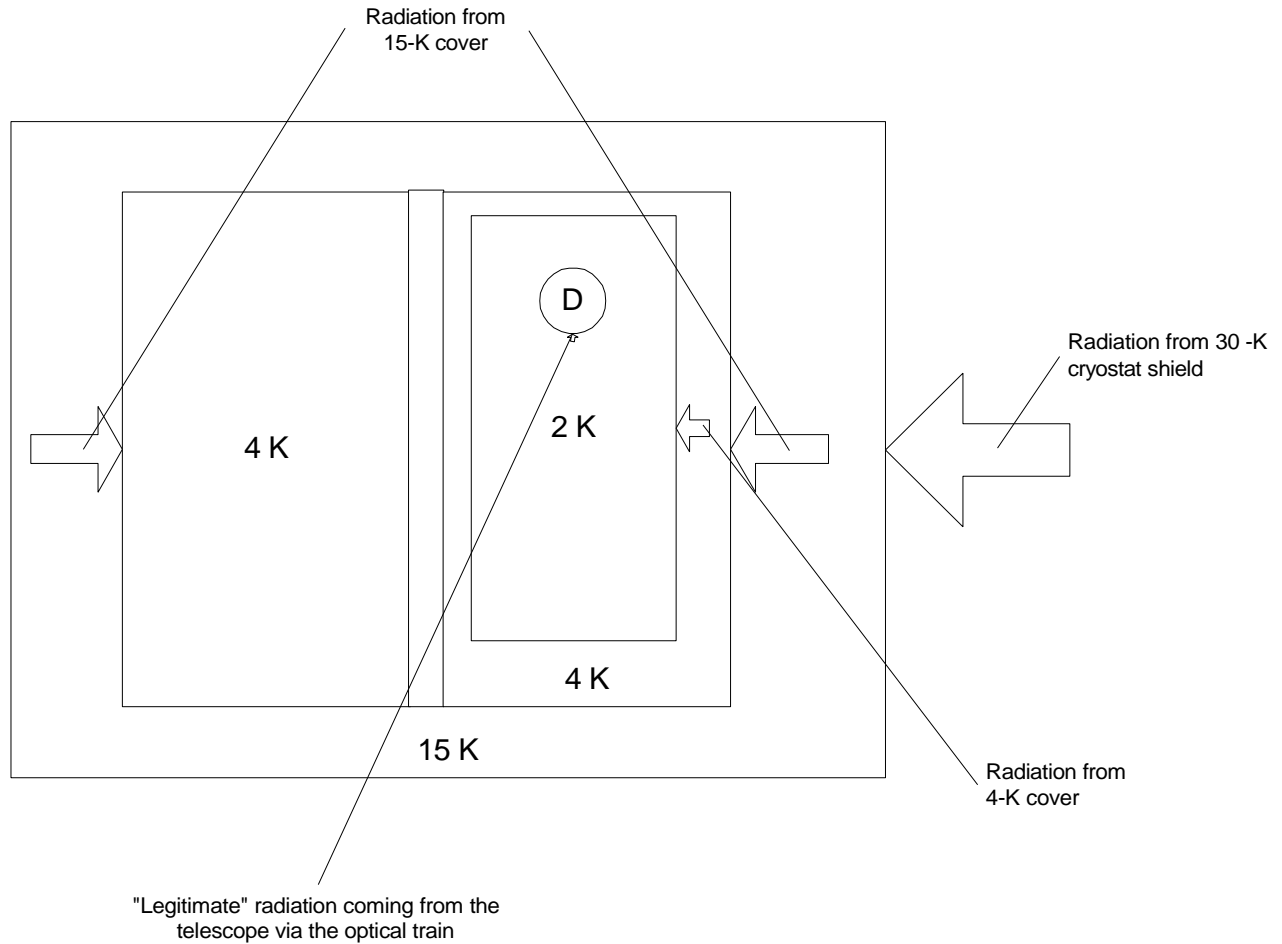


**Figure 5: Illustration of radiation loads from cryostat and instrument covers**

Logo Will Go Here	<b>SPIRE</b>	<b>Ref: SPIRE/RAL/N/</b> <b>Issue: .00</b> <b>Date: 11/12/98</b> <b>Page: 10 of 10</b>
	<b>Possible Conceptual Layout for the SPIRE Structure</b> Author B. Swinyard	

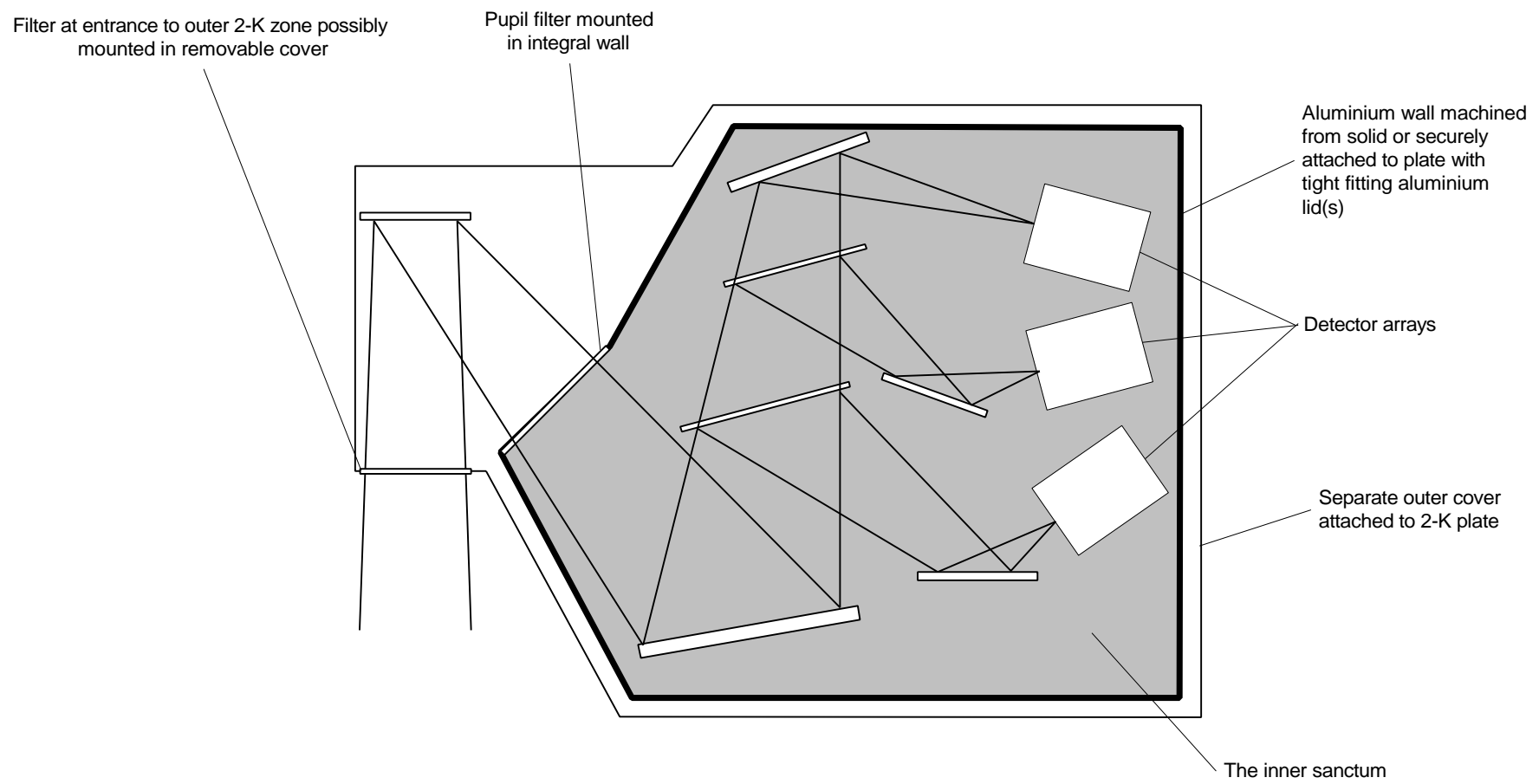


**Figure 6: Rough layout of 2-K photometer components showing position of integral wall and outer cover**

# Minutes of the Warm electronics & S/W working group splinter meeting

Minutes prepared by: Jean-Louis Augeres

**Attendees:** J-L.Auguères (SAp), C.Cara (SAp), R.Cerulli (IFSI), H.Floren (SO), K.King (RAL), G.Olofsson (SO), L.Rodriguez (SAp), L.Vigroux (SAp)

## 1. Introduction:

CCa presented the objectives of the WE&SW working group:

They are:

- Setting up the overall electronics and s/w requirements stemming from various sources as: SPIRE system requirements, IID-A, OIRD, AIV Plan, Detector specifications, PA plan,...
- Define a top level architecture design.
- Participate in the definition and the reviewing of the ICDs between the Electronics & s/w and the other SPIRE sub-assemblies.
- Participate and reviewing of the SPIRE AIV plan.
- Check electronics design and implementation consistency all along the development phase.
- Report to the SPIRE System Team.

## 2. Discussion on WE&SW group membership:

It brought out from the discussions that the group should comprise:

- Permanent members: at least one person from the main labs involved in SPIRE electronics (SAp, IFSI, IAC, SO).
- As circumstances require, other people would be invited to participate: System team member(s), EGSE designer(s), members from other working groups.

## 3. Definition of the Electronics Requirements:

- The setting up of the high level electronics & s/w requirement is regarded as the first priority task.
- Essential inputs are lacking. A first list of these inputs has been discussed and set up during the meeting (see attached list). This list will be submitted to Bruce.

<b>AI-WES-0056-01</b>	Make a fair copy of the essential input list and send it to Bruce (copy to the WE&SW Group)	SAp/ CCa	08/12/98
<b>AI-WES-0056-02</b>	To respond the essential input request list.	BMS	15/01/99



- The SPIRE development plan as well as AIV inputs are considered as essential.
- In house test equipment development have to be taken into consideration.
- The duplication of the AVM has to be considered: one to be delivered, one kept to be used for s/w development and test.

**AI-WES-0056-03** To provide a Development Plan containing AIV information as well KJK 15/12/98

- In parallel of the getting of the essential inputs, the writing of the electronics specifications has to be carried out.

**AI-WES-0056-04** To draft a skeleton of the electronics specifications with the electronics requirements identified so far. Sap/ LR 15/01/99

#### 4. Focal plane simulators.

- G.Olofsson pointed out that his lab cannot afford to provide a focal plane simulator having up to 600 interface lines.
- L.Vigroux stated that such simulator is essential. Its development by the CEA has been envisaged. However, the SPIRE 3 (or 4) simulator (as part of the AVM) should have a much simpler interface (mainly a serial link to the SPU (or DPU)). Proposal will be made.

#### 5. Next meeting.

- The next meeting should take place late January 1999. The main goals of the next meeting will be to review the requirements and the development plan.

**AI-WES-0056-05** To propose a date and a draft agenda for the next WE&SWG meeting. Sap 15/01/99

#### 6. Action list.



**AI-WES-0056-01** Make a fair copy of the essential input list and send it to Bruce (copy to the WE&SW Group) Sap/ CCa 08/12/98

**AI-WES-0056-02** To respond the essential input request list. BMS 15/01/99

**AI-WES-0056-03** To provide a Development Plan containing AIV information as well KJK 15/12/98

**AI-WES-0056-04** To draft a skeleton of the electronics specifications with the electronics requirements identified so far. Sap/ LR 15/01/99

**AI-WES-0056-05** To propose a date and a draft agenda for the next WE&SWG meeting. Sap 15/01/99

	<h1>Note</h1>	 SAp-SPIRE-JLA-xxxx-98 Issue: 1.0 04/12/98
---	---------------	--

**From:** The Warm Electronics & S/W Group.

**To:** B.Swinyard

**Subject:** List of essential inputs required by the Warm Electronics and S/W Working group for the SPIRE warm electronics design

**Action:** To be answered by Jan. 15, 1999

This list has been set up by the Warm Electronics and S/W Working group during a splinter session at the SPIRE Consortium meeting held at RAL on Dec. 2, 1998.

These inputs have been considered as essential. They are the ground of any rewarding work that could be performed by the WE&SW Group.

**Important:** When relevant, detector technology impacts have to be considered.

#### 1. FTS:

- Scan duration
- Sampling rate and accuracy.
- Synchronisation
- Position measurement

#### 2. Chopper:

- Synchronisation
- Position measurement

#### 3. Scan Mode with AOCS:

- Synchronisation
- OBDH time synchronisation

#### 4. On-board dating:

- Resolution / accuracy

#### 5. On-board processing

- Deglitching
- Phase shift on interferograms
- Telemetry rate

## **6. Operating modes:**

- Pick-up
- Parallel mode
- Serendipity

## **7. Degraded modes:**

- reliability requirements
- Scientific priorities (what should we preserve in case of failure: subsystem, telemetry,...)

## **8. Temperature regulation (He<sup>3</sup>)**

## **9. H/K specification (temperature, else)**

- How many
- Accuracy